

Correlated local distortions of the TlO layers in $\text{Tl}_2\text{Ba}_2\text{CuO}_y$: An x-ray absorption study

G. G. Li, F. Bridges

Physics Department, University of California, Santa Cruz, CA 95064

J. B. Boyce

Xerox Palo Alto Research Center, Palo Alto, CA 94304

T. Claeson

Physics Department, Chalmers University of Technology, S-41296 Gothenburg, Sweden

C. Ström, S.-G. Eriksson

Department of Inorganic Chemistry, Chalmers University of Technology, S-41296 Gothenburg, Sweden

S. D. Conradson

MEE-11, Los Alamos National Laboratory, Los Alamos, NM 87545

(April 18, 1994)

We have used the XAFS (x-ray-absorption fine structure) technique to investigate the local structure about the Cu, Ba, and Tl atoms in orthorhombic $\text{Tl}_2\text{Ba}_2\text{CuO}_y$ with a superconducting transition temperature $T_c=60$ K. Our results clearly show that the O(1), O(2), Cu, and Ba atoms are at their ideal sites as given by the diffraction measurements, while the Tl and O(3) atoms are more disordered than suggested by the average crystal structure. The Tl-Tl distance at 3.5 Å between the TlO layers does not change, but the Tl-Tl distance at 3.9 Å within the TlO layer is not observed and the Tl-Ba and Ba-Tl peaks are very broad. The shorter Tl-O(3) distance in the TlO layer is about 2.33 Å, significantly shorter than the distance calculated with both the Tl and O(3) atoms at their ideal $4e$ sites ($x = y = 0$ or $\frac{1}{2}$). A model based on these results shows that the Tl atom is displaced along the $\langle 110 \rangle$ directions from its ideal site by about 0.11 Å; the displacements of neighboring Tl atoms are correlated. The O(3) atom is shifted from the $4e$ site by about 0.53 Å roughly along the $\langle 100 \rangle$ directions. A comparison of the Tl L_{III} -edge XAFS spectra from three samples, with $T_c=60$ K, 76 K, and 89 K, shows that the O environment around the Tl atom is sensitive to T_c while the Tl local displacement is insensitive to T_c and the structural symmetry. These conclusions are compared with other experimental results and the implications for charge transfer and superconductivity are discussed.

PACS numbers: 74.70.Vy, 74.75.+t, 78.70.Dm, 61.70.-r

I. INTRODUCTION

The $\text{Tl}_m\text{Ba}_2\text{Ca}_{n-1}\text{Cu}_n\text{O}_{2(n+1)+m}$ system is a model family of high-temperature superconductors. The structures consist of copper perovskite-like blocks containing n CuO_2 planes (n up to 6 has been observed) separated by one or two TlO layers. Each CaO layer is sandwiched between two CuO_2 layers while the BaO layer is sandwiched between the CuO_2 and TlO layers. For Tl-monolayer ($m=1$) phases, the superconducting transition temperature (T_c) increases to 122 K with the number of CuO_2 planes from $n=1$ to $n=4$ and then decreases with $n=5$ to 6; for Tl-bilayer phases, T_c increases up to 125 K with the number of CuO_2 planes n from 1 to 3 and then decreases with $n=4, 5$. The fully stoichiometric Tl-bilayer $\text{Tl}_2\text{Ba}_2\text{Ca}_{n-1}\text{Cu}_n\text{O}_{2n+4}$ compounds would contain no carriers if the formal ionic valence states, $\text{Tl}_2^{3+}\text{Ba}_2^{2+}\text{Ca}_{n-1}^{2+}\text{Cu}_n^{2+}\text{O}_{2n+4}^{2-}$, are assigned, and thus would not be superconductors. However, there is a hybridization of Tl $6s$ and O $2p$ orbitals which either touch the Fermi surface or cross it [1,2], so the Tl does not act as a completely $3+$ ion and charge transfer might occur between the CuO_2 and TlO layers.

Other effects can also change the hole-doping in the system including: (i) excess or missing O; (ii) Ca^{2+} and/or Cu^{2+} substitution for Tl^{3+} ; (iii) Tl deficiency; (iv) ordering of the O and/or Tl atoms in the TlO layers. Which doping mechanism primarily controls T_c is still an unsolved problem. Structural studies on these compounds will be helpful in understanding the mechanism of superconductivity in this system.

$\text{Tl}_2\text{Ba}_2\text{CuO}_y$ (Tl-2201) [3] is particularly suitable for this study because it has a simple structure (calcium-free and only 1 CuO_2 layer per formula); the highest T_c is about 90 K. The structure of Tl-2201, in fact, has been extensively studied since its first discovery in 1988 [3]. Reasonable agreement for the general structure has been achieved from diffraction studies [4–12]. It contains Tl_2O_2 double layers and a CuO_2 plane separated by a BaO layer, as shown in Fig. 1. For convenience of description, we define the $4e$ site ($x = y = 0$ or $\frac{1}{2}$) as the ideal site for Tl and O(3) in tetragonal $\text{Tl}_2\text{Ba}_2\text{CuO}_y$ and treat orthorhombic $\text{Tl}_2\text{Ba}_2\text{CuO}_y$ to be a pseudo-tetragonal structure. The atomic positions of Tl and O in the Tl_2O_2 double layers, however, are not well defined, due to a large anisotropic thermal factor and/or various static displacements from their ideal sites. Most of the refined structures suggest a distorted site for the O(3) with a displacement of $\sim 0.31\text{-}0.42$ Å along the $\langle 100 \rangle$ direction [4,8,10,11] or $\sim 0.22\text{-}0.28$ Å along the $\langle 110 \rangle$ direction [5,7,9], while some of them show that the Tl atom is also displaced from its ideal site by $\sim 0.11\text{-}0.14$ Å along the $\langle 110 \rangle$ direction [7,9] or ~ 0.16 Å along the $\langle 100 \rangle$ direction [10]. The refined thermal factors in these studies are usually quite large in the ab -plane for the Tl and O(3) atoms. Recently, it has been made clear that the thallium content has a strong influence on the lattice symmetry and thus on the average atomic position in the TlO layer [12–14]. Furthermore, significant distortions have recently been observed in both $\text{Tl}_2\text{Ba}_2\text{CuO}_y$ and $\text{Tl}_2\text{Ba}_2\text{CaCu}_2\text{O}_8$ (Tl-2212) by means of x-ray-absorption fine structure (XAFS) [15]. Similar distortions are found in Tl-2212 by the pair-distribution-function (PDF) analysis of neutron scattering data [16,17]. It appears that these distortions not only have short-range correlations, but may in some cases also have long-range correlations, as evidenced by the presence of the modulational structure for selected sections, observed in high-resolution electron microscopy and electron diffraction [18–22]. In addition, the temperature dependence of the local structure in the CuO_2 plane has been studied by XAFS in Tl-2201 [23,24] and by PDF in Tl-2212 [25], respectively. The splitting of the Cu-O(axial) in $\text{TlBa}_2\text{Ca}_3\text{Cu}_4\text{O}_{11}$ has also been investigated by XAFS in the range $10 < T < 156$ K [26].

In this study, we have focused on the static distortion of the $\text{Tl}_2\text{Ba}_2\text{CuO}_y$, especially in the TlO layer. We have used the XAFS technique [27,28] to probe the local structure around *all* the metal atoms, Cu, Ba, and Tl in $\text{Tl}_2\text{Ba}_2\text{CuO}_y$, to revise the earlier results based on the Tl L_{III} edge studies [15]. Both the sample preparation and the XAFS data analysis are slightly different from the previous study [15]; they are described in Sec. II. The XAFS data analysis (presented in Sec. III) uses constrained fits [29] to reduce the number of independent parameters and to check the previous model. The XAFS data and the data analysis for the Cu and Ba K-edges, and the Tl L_{III} -edge are discussed in Secs. IV and V, respectively. A discussion and a comparison of our results with other experimental observations are given in Sec. VI, and the results summarized in Sec. VII.

II. EXPERIMENTAL DETAILS

A. Sample Preparation and Characterization

Samples of about 10 grams weight were prepared from a mixture of Tl_2O_3 , $\text{Ba}(\text{OH})_2 \cdot \text{H}_2\text{O}$ and $\text{Cu}(\text{NO}_3)_2 \cdot n\text{H}_2\text{O}$, always in the ratio of the cations desired in the final material with no excess of any element. The powders, milled in ethanol and thereafter dried in an inert atmosphere (N_2), were heat treated by a two-step sintering process. The heating rate in both steps was $180^\circ \text{C}/\text{hour}$ and the temperature was regulated by a controller, Eurotherm 818P, with a temperature stability better than $\pm 0.5^\circ \text{C}$.

In sintering step I the mixtures were heated in Al_2O_3 crucibles with Al_2O_3 covers at 760°C for 3 hours with only a limited loss, if any at all, of thallium.

In sintering step II pellets were placed in Al_2O_3 crucibles sealed with gold gaskets and cover. They were subsequently centered in small pieces of ceramic tube and fixed with steel wedges (a procedure that prevents evaporation from the

crucible) and heated at 860° C for 6 hours. The loss of weight in sintering step II, if attributed solely to thallium evaporation, is below 0.3% of the total amount of thallium. There is no sign of substitution of gold into the material or of incorporation of thallium into the gold gasket. From EDX (energy dispersive x-ray spectroscopy) analysis, no traces of Al or Au can be detected in the sample. For estimated errors in barium and copper content see Ref. 12.

Sample purity and lattice parameters were determined from Guinier film data using silicon (NBS 640b) as an internal standard. A computerized photoscanning system in combination with programs for indexing and unit cell refinements were used for the extraction of lattice parameters (a=5.4881(2) Å, b=5.4532 Å, c=23.216(1) Å). The impurity content was below 2%.

Neutron powder diffraction data were collected at the pulsed neutron source ISIS, RAL, UK using the high flux, medium resolution powder diffractometer POLARIS. A least-squares profile refinement program, TF12LS, based on the Rietveld technique was used to analyze the TOF (time-of-flight) neutron powder diffraction data. The refinement was carried out in space group Abma and selected bond distances are found in Tables I-III.

The superconducting properties were studied by ac susceptibility measurements using a Quantum design SQUID magnetometer at temperatures down to 4 K in a field of 50 Gauss. T_c was determined to be 60 K. For further details concerning sample preparation and characterization consult Ref. 12.

B. X-ray absorption measurements

The XAFS samples were prepared by brushing a fine powder ($\approx 30 \mu m$) onto Scotch tape. Each layer was selected to be free of pinholes to minimize the XAFS glitches [30] and several layers were stacked to obtain a sample with a thickness of approximately one absorption length. Samples were measured at 80 K using a liquid-nitrogen dewar. Several data sets were collected for each sample to check for consistency and averaged to improve the signal-to-noise ratio. The x-ray absorption data were collected on beamline 10-2 at the Stanford Synchrotron Radiation Laboratory using Si (400) monochromator crystals. The double monochromator was detuned on its rocking curve to approximately one half of maximum transmitted x-ray intensity to reduce the harmonic content of the beam.

III. XAFS DATA ANALYSIS TECHNIQUE

A. Standard Procedures

The standard procedures for the reduction and analysis of the XAFS data are described elsewhere [27,29]. The extracted XAFS function, $k\chi(k)$, is given by

$$k\chi(k) = \sum_j \frac{N_j F_j(k)}{R_j^2} \sin[2kR_j + \phi_j(k)] \exp(-2k^2\sigma_j^2 - 2R_j/\lambda) \quad (1)$$

where the sum is taken over shells with N_j atoms at a distance R_j from the absorbing atom, k is the momentum of the photoelectron given by $k = [2m(E - E_o)]^{1/2}/\hbar$ where E_o is the energy at one-half the absorption edge height, $F_j(k)$ is the back-scattering amplitude, $\phi_j(k)$ is a phase shift of the photoelectron due to its interaction with the back scattering and absorbing atoms, λ is the effective electron mean free path, and σ_j (Debye-Waller factor) is the average variation (both static and dynamic) of R_j . Examples of the k-space data are given in Fig. 2 for the Cu and Ba K-edges and Tl L_{III} -edge. A Fourier transform of these k-space data exhibits peaks in r-space which correspond to neighbors at different radial distances from the absorbing atom.

To obtain numerical values for R_j , N_j and σ_j , we perform iterated least-square fits of the real and imaginary parts of the Fourier transform of $k\chi(k)$ to a sum of standards over a particular range in real (r) space. Identical k-space transforms are used for the sample and the standards. In these fits, the overlaps of the radial distributions of other neighbors in r-space are included.

It is difficult to extract all the isolated, single pair standards needed for this analysis from other experimental standards. In this study all the standards are generated by the FEFF5 code [31], using a cluster as close to the real lattice as possible with a radius of about 7.5 Å from the central absorbing atom to the boundary scattering atoms. The multiple scattering paths are included in the fit when it is necessary. In earlier studies we have used experimental atom-pair standards extracted from data collected for standard compounds. We have compared our experimental standards with FEFF5 and have obtained very good agreement for about twenty pairs [32]. Since a complete set of experimental standards was not available, we decided, based on our recent study, to use FEFF5 standards. One of the problems in using the standards from FEFF5 is the uncertainty of the amplitude-reduction-factor, S_o^2 . We use two different values of S_o^2 which we have obtained from our detailed comparisons [32]; 0.8 when the back-scattering atom is O, and 0.9 when the back-scattering atom is a metal atom.

B. Background-feature removal

The standard background removal procedure which uses a simple spline or polynomial for $\mu_o(E)$, does not work well when the background consists of some features due to multielectron excitations [33,34] and Ramsauer-Townsend-like effects [34,35]. These features have been found at the Br (in RbBr), Kr, Rb (in RbBr), Ba (in BaO), Ce (in CeO₂), and Pr (in PrBa₂Cu₃O₇) K-edges [33–35] and the Au, Tl (in Tl₂O₃), Pb (in β -PbO₂), and Bi (BaBiO₃) L_{III}-edges [32,33] in our studies. Similar features have also been observed and confirmed by other groups [36–38]. An iterative background extraction and removal procedure has been proposed to obtain and remove these features in the previous work [33].

When the simple standard background removal procedure was applied to the Ba K-edge and Tl L_{III}-edge XAFS data of Tl₂Ba₂CuO_y, spurious humps appear in the low- r region of the Fourier transformed data as shown in Fig. 3. Instead of performing the iterative background removal procedure to these complicated data directly, we utilized the extracted background from the BaO [35] and Tl₂O₃ [32] data; the new background was obtained by fitting the corresponding extracted background plus simple spline functions to the data. These new backgrounds are plotted in Fig. 3. They contain more wiggles than the background obtain from the standard procedure but result in smoother r -space data in the low- r region than those from the standard procedure. This simple method works very well. We note that using more spline sections in the standard procedure may also minimize the humps in the low- r region but that usually reduces the amplitude of the first r -space peak, simultaneously.

C. Constrained Fits

One of the common problems in the XAFS data analysis is that there are too many fitting parameters if the fit includes further shells in a complicated system. For example, if the fitting range is 3.0 ~ 13.0 Å⁻¹ in k -space and 1.0 ~ 4.0 Å in r -space, the *estimated* allowed number of fitting parameters is ~21, according to the formula $2\Delta k\Delta r/\pi + 2$ [39]. In a complicated system, such as the Cu edge data in YBa₂Cu₃O₇ [29,40,41], the number of atomic pairs could exceed 8, which needs 24 or more fitting parameters, even if all the E_o ' are fixed and not considered as fitting parameters. Therefore, a constrained fit is required in the XAFS data analysis for a complicated system. These constraints include using the lattice constants and the known average locations of the atoms in the unit cell from diffraction measurements, combining the XAFS results viewed by different atoms, and using equations which relate a parameter to one or more other parameters (for examples, keeping the ratio of some parameters constant; setting a parameter to the weighted sum of other parameters) to check possible models. The constraints force the fit towards a particular minimum in parameter space, and the fit is not easily trapped in some other local minima. In this way, the constrained fits can help reject results which are physically inconsistent and to check particular models for the local structure. This method has been used to a limited extent in our earlier work [40,41] and more extensively in our recent studies [29].

IV. XAFS DATA PRESENTATION AND QUALITATIVE FEATURES

A. Cu environment

From diffraction studies [4–12], the average local environment about a Cu atom is as follows: 4 O(1) neighbors at $r=1.93$ Å in the CuO₂ plane, 2 O(2) neighbors at 2.71 Å along the *c*-axis, 8 Ba neighbors at 3.35 Å above and below the CuO₂ plane, and 4 Cu neighbors at 3.87 Å in the CuO₂ plane. In XAFS data, the Fourier transform of the XAFS function $k\chi(k)$ to real (*r*) space is a sum of peaks corresponding to each of these different neighbors; however, each distance is the average local value, not necessarily the value calculated from the average unit cell. The question considered in this section is how well does the Cu local environment agree with diffraction results.

The Cu K-edge XAFS data in *r*-space are shown in Fig. 4. The transform range is a square window from 3.1 to 16.5 Å⁻¹, Gaussian broadened by 0.3 Å⁻¹. Both the real part and the magnitude of the complex transform are plotted. The distances between the absorbing atom and the back-scattering atoms are determined by the phase of the XAFS function, which is well represented by the positions of the zero-crossing points of the real and imaginary parts of the Fourier transform. However, there is a shift, $-0.2 \sim -0.5$ Å, of the XAFS peaks from the real positions due to the photoelectron phase-shifts.

To compare the local structure which determines the Cu K-edge XAFS with the average structure obtained from diffraction, we generated the theoretical XAFS function using FEFF5 [31] and the refined crystal structure obtained from diffraction measurements [4]. In the calculation, all the atoms within a distance of 7.5 Å from the central absorbing atom, and all the scattering paths with a contribution of 4% or more, relative to the maximum contribution, are included. To roughly simulate both the static and thermal disorder in the calculation, we have set the sample temperature to 100 K and the Debye temperature to $700(\text{K Å})/(0.5R_j)$ which increases σ with distance R_j for more distant shells. (The same thermal parameters are used for the other edges in this paper unless noted). The Fourier transform of the theoretical XAFS (without any fitting) is shown in Fig. 4 by dotted lines, with the same *k*-space window as for the experimental data, an overall amplitude-reduction-factor of 0.9, and an overall E_o shift of -2.0 eV.

Fig. 4 shows that the phase of the theoretical XAFS agrees very well with that of the experimental data up to 6.5 Å. This means that the O(1), O(2), Ba, and Cu atoms are well ordered about a given Cu atom, in excellent agreement with the diffraction results. We point out that the Cu edge XAFS data is not sensitive to the distortion of the distant TlO layers if there is any, especially when the distortion is in the *ab*-plane, because the TlO and CuO₂ layers are separated by 4.7 Å and a small splitting of the Cu-Tl and/or O(3) distances can be absorbed by a large Debye-Waller factor. We note that the subtle differences in zero-crossing points are due mainly to the errors in E_o , especially in the region below 2.3 Å where the O atoms make a major contribution. The nearest O neighbors directly touch and partially screen the excited absorbing atom which has a hole in the core-shell level, thus the E_o shift for the nearest O neighbors should be different from the distant neighbors. Since the same E_o shift is used for all neighbors in the simulation, an error in the phase-shift can be introduced in the first O peak. The discrepancy in the magnitude is mainly from the rough estimation of the Debye-Waller factors and the amplitude-reduction-factors of the XAFS function in the theoretical calculation and is not strongly related to the separations of the atomic pairs.

We emphasize that in the theoretical calculation we did not adjust the XAFS parameters, N_j , R_j , σ_j , and E_{oj} , individually; instead, we only adjusted the overall amplitude and E_o and simulated the Debye temperature of the different pairs by a simple formula. This method makes it possible and easy to compare the experimental XAFS data with a theoretical function calculated for a particular model up to 7 Å (for example, from the refined average unit cell obtained from diffraction). However, it is still difficult to make a detailed fit to the experimental XAFS data much beyond 4 Å.

B. Ba environment

The Ba atom is in a plane between the CuO₂ and TlO layers. From diffraction measurements [4–12], it has 4 O(1) neighbors at 2.73 Å, 4 O(2) neighbors at 2.84 Å, 1 O(3) neighbor at 3.00 Å, 4 Cu neighbors at 3.35 Å, 5 Ba neighbors

(4 in the ab-plane and 1 along the c-axis) near 3.86 Å, and 4 Tl around 3.9 Å [4]. Again we ask the question if the local structure about the Ba atoms is the same as that given by the diffraction results assuming no distortions of the Tl atoms. The Fourier transform of $k\chi(k)$ for the Ba K-edge data is shown in Fig. 5; window is from 3.5 Å⁻¹ to 15.5 Å⁻¹, Gaussian broadened by 0.3 Å⁻¹. We have generated the theoretical Ba XAFS function following the procedure described earlier for the Cu edge; it is plotted as dotted lines in Fig. 5a.

The phase of the theoretical and experimental XAFS function agreed very well up to 3.7 Å (a small discrepancy in the phase of the first peak can be easily minimized by using a different E_o shift). This again indicates that the O(1), O(2), Cu and Ba atoms are well ordered. Similarly, there is excellent agreement in the phase for a large peak around 5.2 Å between the simulation and experimental XAFS data. The dominant contributions to this peak arise from the collinear, forward, multiple scattering of the Ba-O(1)-Ba and the multiple scattering of intraplanar Ba-O(2)-Ba pairs. The phase of the real part of the transform within the 5.2 Å peak is shifted by nearly $\pi/2$ relative to the phase that would be observed for a single scattering Ba-Ba peak (*e.g.* as occurs near 3.5 Å in Fig. 5) due to the forward multiple scattering contributions. The good agreement between the calculations and the experimental data for this peak strongly suggests that the Ba atom is well ordered.

More importantly, however, there is a significant difference between the calculations and the experimental data on the high-r side of the peak near 3.6 Å (see Fig. 5c in which a small fraction of the data is shown with an enlarged x -axis), where the Ba-Tl pair ($r=3.90$ Å) should make a major contribution. The experimental data in this region of r-space can be simulated much better by FEFF5 when the Ba-Tl pairs are excluded; *i.e.*, the net Ba-Tl peak is small. This means that the Ba-Tl peak is either very broad due to disorder of the Tl atoms or is split into multi-peaks due to a displacement of the Tl atom from its ideal site.

C. Tl environment

There are two adjacent TlO layers, which are surrounded by two BaO layers, one above and one below. The average local structure around the Tl atoms obtained from diffraction [4–12] consists of 1 O(2) and 1 O(3) atoms near 2.0 Å, 4 O(3) within 2.3–3.2 Å; 4 interplanar Tl atoms near 3.5 Å and 4 intraplanar Tl atoms near 3.9 Å; and 4 Ba atoms near 3.9 Å. However as outlined in the introduction and the above discussion at the Ba edge, there is considerable evidence that the TlO layers are distorted. Here we investigate this disorder using Tl edge XAFS data.

First, we performed a multiple-scattering-cluster-simulation for the Tl L_{III}-edge XAFS (as described above for the Cu K-edge data) assuming the structure of Ref. 4 in which the Tl is at the ideal 4e site while the O(3) is displaced along the $\langle 100 \rangle$ direction by 0.37 Å from its ideal 4e site. Both the simulated and experimental XAFS, $k\chi(k)$, were Fourier transformed to r-space using a k-space range of 3.2 - 15.5 Å⁻¹, Gaussian broadened by 0.3 Å⁻¹, as shown in Fig. 6a. In the simulation, we used two different sets of Debye-Waller temperatures, 300 (K Å)/(0.5 R_j) for Tl-Tl pairs and 700 (K Å)/(0.5 R_j) for other pairs, to better simulate both the static and thermal disorder. This gives a good simulation above 4.5 Å in r-space.

Significant differences in the phase between the simulated and experimental data are observed in Fig. 6a. Thus at least some of the distances derived from the average, crystallographic structure are not consistent with these XAFS data. For the first O neighbor peak (1.3–2.3 Å in Fig. 6) of the simulated data, the phase of the low-r side (1.3–1.8 Å), where the Tl-O(2) and Tl-O(3) pairs at $r=2.0$ Å make their major contributions, agrees reasonably well with the experimental data; however, at the high-r side of this peak (1.8–2.3 Å), where the Tl-O(3) pair at $r=2.5$ Å makes its major contribution, the phase is not consistent with the experimental data and a contribution in the simulated data is missing in the experimental data. A comparable inconsistency is observed in the peak centered near 3.6 Å. The phase and the shape of the simulation for this peak agree well with the actual data in the low-r side, where the interplanar Tl-Tl pair makes its major contributions; however, it does not agree in the high-r side (3.7–4.0 Å), where the intraplanar Tl-Tl and also the Tl-Ba pairs make their major contributions. Furthermore, the amplitude of the simulated peak in r-space near 3.6 Å is almost twice as big as that in the data. This discrepancy is too large to be explained just by the errors in the amplitude-reduction-factor and the Debye-Waller factors. This implies a

significant distortion and/or disorder in the Tl-Tl and Tl-Ba distances from the average distances obtained from the refined structure in diffraction. A simulation without the intraplanar Tl-Tl pairs bears a much closer resemblance to the experimental spectra near 3.5 Å. These comparisons again suggest that the Tl atoms, and probably also the O(3) atoms, occupy more distorted sites in the ab-plane than those obtained from the average diffraction experiments.

V. DETAILED XAFS DATA ANALYSIS

From the qualitative analyses of the Cu, Ba, and Tl edge XAFS data shown above, we conclude that the positions of the Cu, O(1), O(2), and Ba atoms in the unit cell are consistent with the average crystallographic structure obtained from diffraction studies. However, the Tl and O(3) atoms are significantly more distorted than the average structure obtained in many diffraction studies. The XAFS data indicate that these distortions are located in the ab-plane of the TlO layer as suggested in some diffraction investigations. These qualitative features are model independent and give a sound guidance for further structural analysis.

In this section, we will perform nonlinear-least-square fits to the XAFS data to further check the qualitative features shown above and gain quantitative information on the local structure about the Cu, Ba, and Tl atoms.

A. Cu environment

The r-space Cu K-edge XAFS data have been fit up to 3.9 Å using individual standard atomic pairs generated by FEFF5. Five pairs are included in the fit: Cu-O(1) near 1.9 Å, Cu-O(2) near 2.7 Å, Cu-O(1) near 4.3 Å, Cu-Ba near 3.4 Å, and Cu-Cu near 3.9 Å in which the multiple-scattering-paths for Cu-O(1)-Cu are included. The experimental data and the fit are shown in Fig. 7, where the same Fourier transform range is used as in Fig. 4 and the fitting range is between 1.0-3.9 Å. Overall, a high quality fit has been achieved. A double-well potential was used in Ref. 23 to improve the fit for the first Cu-O(1) peak; however, in this study, the refinement of the first peak is not important and we use only a single Cu-O(1) peak. The structural parameters extracted from the XAFS curve-fitting are tabulated in Table I, together with the results from diffraction refinement. Our XAFS results are in excellent agreement with the diffraction results, as expected from our earlier comparison of the simulated and experimental XAFS r-space spectra, in which there was an excellent phase agreement up to 6.7 Å. These XAFS results are also very close to the previous results [42].

B. Ba environment

In Sec. IV, we showed that the Tl is disordered or distorted. So in the fits to the Ba K-edge data, we considered three situations for comparison: (1) no Ba-Tl peak, (2) a single Ba-Tl peak, and (3) a split Ba-Tl peak. For the first case, we fit the Ba K-edge XAFS data with 3 O peaks (at $r=2.7$ Å, 2.8 Å and 3.0 Å, respectively), 1 Cu and 1 Ba peak. The Tl peak near $r=3.9$ Å was not included. The Debye-Waller factor of the Ba-Cu peak was fixed to have the same value as that of the Cu-Ba peak from the Cu K-edge fit. A reasonably good fit is achieved and all the extracted parameters are reasonable, which means that the Ba-Tl pairs do not make a significant contribution to the Ba edge XAFS, in contradiction to what one would expect for the undistorted Tl layers.

Secondly, we included the Ba-Tl peak in the fit and fixed the amplitude of that peak to 4, the number predicted by diffraction. The quality of the fit was improved by about 25% and the extracted distances and the amplitudes for the Ba-O, Ba-Cu and Ba-Ba peaks remained essentially unchanged. The Ba-Tl distance is about 3.90 Å, very much the same as the average distance given by diffraction. The Debye-Waller factor of the Ba-Tl peak is about 0.094 Å, much bigger than that of the Ba-Ba peak (0.066 Å).

Finally, we tested the model proposed earlier [15]. Here we require consistency between the XAFS spectra collected from three different absorbing atoms, achieved by using constraints in the fitting procedure. Following our previous

discussion, we assumed that the Tl atoms are shifted along $\langle 110 \rangle$ so that the 4 Ba-Tl pairs split into three distances, with roughly 1 pair at $r - \delta r$, 2 pairs at r and 1 pair at $r + \delta r$. Therefore, we included 3 O, 1 Cu, 1 Ba and three Ba-Tl peaks in the fit. To minimize the number of fitting parameters and to check the model, we fixed the average distance r and the amplitudes of these three peaks to the values predicted by the model and only allow δr to vary for these Ba-Tl peaks. The Debye-Waller factors of the three Ba-Tl peaks and the E_o shifts for the same type of back-scattering atoms were also kept equal. In this way, the number of the variables was reduced to 18, well below 23, the estimated number of allowed variables obtained from $(2\Delta r \Delta k / \pi + 2)$ [39]. The quality of the fit and the extracted parameters for O, Cu and Ba peaks are essentially the same as the fit with a broader Ba-Tl peak but here $\delta r = 0.10 \text{ \AA}$. As a final step, we also allowed the average Ba-Tl distance and the amplitudes of the Ba-Ba and Ba-Tl peaks to vary. The final fitting parameters remained essentially the same as the ones with the strong constraints.

The experimental spectra and the final fitting curves are plotted in Fig. 8a; the contributions from O, Cu and Ba atoms are shown in Fig. 8b, while the contributions from the split Ba-Tl pairs are shown in Fig. 8c. These results clearly show that the contributions of the Ba-Tl pairs are quite small compared to the Ba-Cu and Ba-Ba pairs. The detailed results are listed in Table II, together with the results from diffraction and the model for comparison. We would like to point out that the Ba-O(3) distance is not sensitive to the displacement of the O(3) atom in the ab -plane. For Ba-Tl peaks, δr is slightly coupled with the Debye-Waller factor σ and the coordination number N . It varies from 0.08 \AA to 0.11 \AA depending on σ and N (or S_o^2). We also used different k weighting (*i.e.*, $k^n \chi(k)$ with $n=1, 2, 3$) and different k ranges for the Fourier transform in the fit. The derived parameters are essentially the same within the estimated uncertainty. In all cases, the splitting distance, δr , for the Ba-Tl pair is significantly shorter than 0.2 \AA , the distance predicted by the previous model. This means the displacement of the Tl atom in the previous model (0.28 \AA) is too large and has to be modified to fit the Ba edge XAFS data.

We also simulated the Ba K-edge XAFS data with a distorted model for the TlO layer. Here we modified the previous model by assuming that the Tl atom is displaced 0.11 \AA from its ideal site along the $\langle 110 \rangle$ direction. The simulated data are plotted in Fig. 5b. The agreement with the data is much improved for the r -space range $3.5\text{--}4.5 \text{ \AA}$ compared to the earlier simulation (Fig. 5a), as illustrated in Fig. 5c. There is also improved agreement in phase near 6 \AA .

C. Tl environment

From the analysis of the Cu and Ba K-edge XAFS spectra, we conclude that the O(1), O(2), Cu, and Ba atoms are at their ideal sites in the unit cell just as diffraction shows, but the Tl atom is shifted from its ideal site. However, it is difficult, from the Cu and Ba edge XAFS spectra only, to distinguish between a randomly disordered Tl site (which gives a broad peak) and a distorted Tl site (which gives multiple peaks) and hence to derive the actual displacement of the Tl atom if it is at a distorted site. Further information from the Tl edge is desirable.

The Tl L_{III} -edge XAFS data are more sensitive to the Tl distortion, but the data analysis is more complicated by the fact that there are two adjacent TlO layers. In the fits to the Tl edge data, we considered the Tl displacements along the $\langle 110 \rangle$ direction with two different magnitudes: (1) $\sim 0.3 \text{ \AA}$, similar to the previous model [15], and (2) $\sim 0.1 \text{ \AA}$, as suggested by the Ba edge XAFS data. In comparisons with diffraction studies, we also tried other models, see Sec. VI.A.

In order to enable a meaningful analysis of the Tl L_{III} -edge data we treat the Tl atoms as if they all see the same local distortions. However, we know that in the related Bi-based cuprate superconductors, there exist strong periodic modulations [43] which result in superstructure with long range order, a buckling in the ab -plane, and periodically extra O atoms. Because diffraction results show little disorder for Tl along the c -axis, we are motivated to use a simple model for the local environment. As discussed later, it is still compatible with a superstructure unit cell.

We first performed a rough fit to the data in the region of $1.3\text{--}3.8 \text{ \AA}$, with 2 O, 1 Tl and 1 Ba peaks, similar to the model used in the previous paper [15]. The extracted structural parameters are the following: 1.8 O atoms at 2.04 \AA , 2.9 O atoms at 2.35 \AA , 2.8 (which is too small compared to 6) [44] Tl atoms at 3.51 \AA , and 7.6 Ba atoms (but very

broad, with $\sigma = 0.13\text{\AA}$) at 3.89\AA . This shows that the interplanar Tl-Tl pair (at $r=3.5\text{\AA}$) remains but the intraplanar Tl-Tl pairs (with an average distance of 3.9\AA) do not make a large contribution to the Tl edge XAFS spectra as would occur for an undistorted site. This result suggests that the Tl atom is distorted (not randomly disordered) in a particular way so that the interplanar Tl-Tl peak remains but the intraplanar Tl-Tl peak seems to disappear. The fitting result we obtain here is quite close to the earlier result [15]. However, the model based on that result requires a large shift for the Tl atom which does not fit the Ba edge data as discussed above, and the Tl-Tl amplitude is too low. Therefore, the previous model must be modified to fit both the Ba and Tl edge XAFS data.

Secondly, we followed the previous model but with a smaller shift for the Tl atom. Assuming that the Tl atoms are shifted along the $\langle 110 \rangle$ direction as shown in Fig. 9, the interplanar Tl-Tl distance remains approximately unchanged while the intraplanar Tl-Tl distance splits into two distances. In addition, the Tl-Ba distance splits into three distances, with the average distance unchanged to first order. In order to check this model more carefully, we explicitly included all the split peaks and the long Tl-O peak at 4.3\AA in the fit using the constrained-parameter technique. The numbers of neighbors for all the Tl and Ba peaks are fixed to the values predicted by the model. The average Tl-Ba and intraplanar Tl-Tl distances are also fixed to the average distances given by the diffraction measurement, and only the split distances are allowed to vary. The Debye-Waller factors of the three Tl-Ba peaks are set to be equal to those of the Ba-Tl peaks at the Ba edge, to further reduce the number of independent variables and to check the consistency of the fitting results. The E_o shifts for the same type of back-scattering atoms are kept equal except for the nearest O atoms. Thus the total number of variables is 16, far below the estimated number of allowed variables, 27 [39]. The fit was carried out in the region of $1.2\text{\AA} < r < 4.2\text{\AA}$, with the Fourier transform range of $3.3\text{\AA}^{-1} \sim 15.5\text{\AA}^{-1}$, Gaussian broadened by 0.3\AA^{-1} . A high quality fit was achieved.

Finally, we allowed the average Tl-Ba and intraplanar Tl-Tl distances, the amplitudes, and the Debye-Waller for the three Tl-Ba pairs to vary. The fitting results remained essentially the same as those with the constraints. We also fit the data with different k weighting ($k^n \chi(k)$, $n=1, 2, 3$) and k range in the Fourier transform. Consistent results were achieved within the estimated uncertainty.

The final fit is shown in Fig. 10a. The contributions from O, Tl and Ba atoms are plotted in Fig. 10, b-d, respectively. The contributions from the three individual Tl-Tl peaks are plotted below the sum of their contributions. The contribution of the Tl-Tl at $r=4.02\text{\AA}$ is small, and the Tl-Tl peak at $r=3.72\text{\AA}$ is out of phase with the Tl-Tl peak at $r=3.50\text{\AA}$, resulting in partial destructive interference. Thus the sum of the Tl-Tl peaks has almost the same phase as that of the Tl-Tl peak at $r=3.50\text{\AA}$ but a smaller amplitude, which explains why the fit with only one Tl-Tl peak gives quite good agreement, but with a small amplitude. The three Tl-Ba peaks are also plotted below the sum of their peaks. The sum of the three split Tl-Ba peaks is a broad peak, with a similar phase to that of the Tl-Ba peak at the average diffraction distance, 3.90\AA , which again is consistent with one broad Tl-Ba peak in the previous fit.

The extracted structural parameters are listed in Table III, together with the corresponding parameters calculated from the model. We emphasize that the Tl-Ba distances obtained in this new fit of the Tl L_{III} -edge data are in good agreement with the Ba-Tl distances extracted from the Ba edge XAFS data within the estimated uncertainty. In the model, we only shifted the Tl atom along the $\langle 110 \rangle$ direction to match the Tl-Tl, Tl-Ba and Ba-Tl distances extracted from our XAFS data. The best overall agreement is achieved when the Tl atom is displaced by about 0.11\AA . We have also shifted the O(3) atom along the $\langle 100 \rangle$ direction from the $4e$ site by 0.53\AA in the model to match the observed average interlayer Tl-O distance at 2.33\AA . The splitting of the two shorter interlayer Tl-O distances ($r=2.29$ and 2.38) predicted by the model is consistent with the broad Tl-O peak ($\sigma=0.131\text{\AA}$) at $r=2.33\text{\AA}$ in the data. We point out that absolute position for the O(3) is not well defined in the data because the Tl-O peak at 2.33\AA is quite broad and the Tl atom itself is displaced. The long interlayer Tl-O(3) peak, predicted to be near $r = 3.12\text{--}3.24\text{\AA}$ by the model, is not clearly observed in the XAFS data, probably because that peak is considerably broader than the shorter one, and/or smeared out due to multiple Tl-O peaks in that range. Instead of the well defined pair distances predicted by the model, the actual PDF of the Tl-O(3) pairs within the TlO layer may be spread over the entire range $2.3\text{--}3.2\text{\AA}$ (refer to Table III) due to the variations of the Tl and O(3) displacements in both magnitudes and directions.

We again simulated the Tl edge XAFS, using the FEFF5 code and the distorted local structural model (see Fig.

9). The simulation is shown in Fig. 6b. The sample temperature and Debye-Waller temperature used here are the same as those used in the simulation shown in Fig. 6a, except the parameters for the first two Tl-O pairs ($r=2.00$ Å and 2.09 Å) in which the Debye-Waller factors were set to 0.03 Å because the static disorder had already partially been taken into account by the two separated peaks. The new simulation in Fig. 6b shows a great improvement over the old one shown in Fig. 6a, and the phase of the new simulation agrees very well with the actual data over the whole region.

VI. DISCUSSION

A. Comparisons with diffraction results

The extracted distances from our XAFS data analyses for the undistorted atomic pairs, such as Cu-O, Cu-Ba (Ba-Cu), Cu-Cu, Ba-O(1,2), Ba-Ba, are in excellent agreement with those obtained from diffraction studies, with a typical error of 0.01 Å (see Table I and II). This shows the high quality of the XAFS data and the data analyses. The extracted distances for the distorted atomic pairs, such as Ba-O(3), Ba-Tl (Tl-Ba), Tl-O, are within the range of the distances given by diffraction investigations (see Table II and III).

Diffraction studies [4,7–9,11] show that the refined thermal factors for the Tl and O(3) atoms along the c -axis are only one third or less of those in the ab -plane. Therefore, we did not attempt to vary the c -components of the Tl and O(3) positions in our model; they are fixed at the average positions given by diffraction studies. Furthermore, the mean-square-root of the Tl displacement is about 0.15 Å in the ab -plane ($\sqrt{U_{11}}$ or $\sqrt{U_{22}}$) and 0.09 Å along the c -axis ($\sqrt{U_{33}}$) in the refinement of diffraction studies [4,7–9,11], which are quantitatively consistent with our XAFS results. Given the Tl displacement of 0.11 Å in the ab -plane and the Tl Debye-Waller factor of 0.09 Å (see Table III), the approximately estimated mean-square-root of the Tl displacement in the ab -plane is 0.14 Å ($\sqrt{0.11^2 + 0.09^2}$ Å), very close to that of the diffraction results.

The model (Fig. 9) based on our XAFS data analyses suggests that the Tl displacements are correlated over a short range. The partial-pair-distribution-function (PPDF) for the Tl-Tl pairs extracted from our data shows a dip near the average distance as shown in Fig. 11a, which is significantly different from the Tl-Tl PDF for the Tl in the ideal sites as shown as the dotted curve in Fig. 11b (with a Debye-Waller factor 0.07 Å). The second peak in the ideal structure is split into two peaks in the extracted PDF, one near 3.7 Å and another one near 4.0 Å, thus a dip is introduced near the average distance 3.87 Å. When we fit the data using the ideal structural model (4 Tl-Tl at 3.51 Å, 4 Tl-Tl at 3.87 Å and 4 Tl-Ba at 3.89 Å), the longer Tl-Tl pair is moved to 3.75 Å (solid curve in Fig. 11b) which physically does not make sense because the average Tl-Tl distance in the ab -plane should equal to the average lattice, 3.87 Å.

Our model is similar to that suggested by the PDF analysis of the pulsed-neutron scattering spectrum in Tl-2212 [16,17], but more specific about the relative shift for the Tl atoms between the two consecutive TlO layers. Since the interlayer Tl-Tl distance remains unchanged, the displacement of the nearest Tl-Tl pairs between the TlO layers should be either in the same direction or perpendicular to each other, but not in opposite directions. The shifts of the Tl and O(3) atoms and the pair distances obtained from XAFS, however, are different from those obtained by PDF even if the small changes in the lattice constants between Tl-2201 and Tl-2212 are taken into account. The PDF analysis for Tl-2212 suggests that the Tl atom shifts by 0.32 Å along the $\langle 110 \rangle$ direction, which results in three split Tl-Ba distances with $\delta r \simeq 0.23$ Å. This is not consistent with our Ba K-edge XAFS data ($\delta r \simeq 0.1$ Å). We point out that XAFS probes the local environment around each selected element separately, and thus determines the average local structure around every different element. The combination of the information from different types of absorbing atoms gives a more constrained result for the local structure. On the other hand, PDF analysis uses all the atomic pairs in the material together, so that identifying individual partial pair-distribution-functions (PPDFs) is a much more involved process. Consequently, XAFS offers an advantage in studying the near neighbor local structure around an absorbing atom in complicated materials.

Some diffraction studies also revealed a Tl displacement from its ideal site [7,9,10]. An x-ray structural study of tetragonal single crystals $(\text{Tl}_{1.85}\text{Cu}_{0.15})\text{Ba}_2\text{CuO}_6$ with $T_c=110$ K suggested that the Tl is displaced along the $\langle 110 \rangle$ direction by 0.11 \AA [9]. Another x-ray diffraction study on tetragonal single crystals $\text{Tl}_{1.87}\text{Ba}_2\text{Cu}_{1.13}\text{O}_{6+\delta}$ with $T_c=12$ K showed a Tl displacement of 0.16 \AA along the $\langle 100 \rangle$ direction [10]. A neutron powder diffraction investigation of orthorhombic $\text{Tl}_2\text{Ba}_2\text{CuO}_{6+\delta}$ with $T_c=90$ K inferred a Tl displacement of 0.14 \AA along the b -axis [7] (which is along the $\langle 110 \rangle$ direction in a tetragonal unit cell). In all these diffraction studies, the Tl atoms are assumed to be statistically distributed in the displaced sites. This leads to an uncorrelated Tl displacement with the Tl-Tl PDF having its largest amplitude at the average distance (see dotted lines in Fig. 11b and c), which is significantly different from the PPDF proposed by our XAFS study. To further check the models suggested by diffraction studies, we have tried to fit the XAFS data with the uncorrelated Tl displacement model for displacements along both the $\langle 110 \rangle$ and $\langle 100 \rangle$ directions.

1. Tl displacement along the $\langle 110 \rangle$ direction

In the $\langle 110 \rangle$ direction Tl displacement model suggested by one diffraction study [9], the four-fold displaced sites of the Tl are randomly occupied. Thus, to check that model in the XAFS data analysis, eight Tl-Tl pairs must be included in the fit with distances $r_1 - 2\delta r_1$, $r_1 - \delta r_1$, r_1 , $r_1 + \delta r_1$, $r_1 + 2\delta r_1$, $r_2 - 1.9\delta r_1$, r_2 , $r_2 + 1.9\delta r_1$ and amplitudes 0.25, 1, 1.5, 1, 0.25, 1, 2, 1, respectively. Here, r_1 and r_2 are the average Tl-Tl distances between and within the TlO layers, respectively; the splitting of the Tl-Tl distances from their average distances are proportional to δr_1 to first order. Correspondingly, three Tl-Ba pairs must be included in the fit with distances $r_3 + \delta r_3$, r_3 , $r_3 - \delta r_3$ and amplitudes 1, 2, 1, respectively. Three Tl-O pairs near 2.0 \AA , 2.3 \AA and 4.4 \AA were also included.

The fit was started with the Tl displacement of 0.11 \AA from its ideal site (which corresponds to $\delta r_1=0.085 \text{ \AA}$ and $\delta r_3=0.08 \text{ \AA}$) and Debye-Waller factors of 0.07 \AA for the Tl-Tl and Tl-Ba pairs. The starting Tl-Tl PDF is shown in Fig. 11b as dotted line. To reduce the number of fitting parameters and to check the proposed model, we fixed r_1 , r_2 , and r_3 at the average distances (3.51 \AA , 3.87 \AA , and 3.89 \AA , respectively) given by diffraction study, and the amplitudes of the Tl and Ba peaks to the numbers predicted by the model. The E_o shifts for the same type of back-scattering atoms are kept equal except for the nearest O atoms. With these constraints, the total number of variables is 25 for this 14-pair-fit. The fitting range is exactly the same as that used for the correlated model (Sec. V.C).

The extracted PPDF is plotted in Fig. 11c as the solid line. The quality of this fit with 25 parameters is comparable to the one obtained from the constrained fit using the correlated model (Fig. 9) with only 16 variables. The distances changed a little from the starting values to $\delta r_1=0.095 \text{ \AA}$ and $\delta r_3=0.07 \text{ \AA}$. Since the weighted number of the Tl-Tl pairs are fixed, their Debye-Waller factors are varied to adjust the height of the peaks. The extracted Debye-Waller factors are less than 0.04 \AA for the Tl-Tl peak at 3.51 \AA and larger than 0.2 \AA for the Tl-Tl peak at 3.87 \AA , which results in a sharp peak at 3.51 \AA and a dip near 3.87 \AA in the Tl-Tl PDF as shown in Fig. 11c by the solid line. For the Tl-Ba PDF, there is no difference between the $\langle 110 \rangle$ direction correlated and uncorrelated Tl displacements, and the extracted Tl-Ba PDFs are very similar.

Although the quality of the fit for the uncorrelated model (25 variables in the fit) is comparable to that of the correlated model (16 variables in the fit), the extracted Tl-Tl PDF (solid line in Fig. 11c) from the constrained fit is significantly different from the starting Tl-Tl PDF (dotted line in Fig. 11c) which corresponds to the uncorrelated model. Furthermore, the extracted Tl-Tl PDF appears to be very close, within the imposed constraints, to that obtained from the correlated displacement model (solid line in Fig. 11a); *a dip shows up at the average distance 3.87 \AA . For the uncorrelated model, a peak must show up at the average distance in the Tl-Tl PDF.* Clearly, our XAFS data do not support the uncorrelated $\langle 110 \rangle$ Tl displacement model.

2. Tl displacement along the $\langle 100 \rangle$ direction

For the $\langle 100 \rangle$ direction uncorrelated, four-fold Tl displacement model suggested by diffraction study [10], eight Tl-Tl pairs must be included in the XAFS fit with distances $r_1 - \delta r_1$, r_1 , $r_1 + \delta r_1$, $r_2 - 1.77\delta r_1$, $r_2 - 0.885\delta r_1$, r_2 , $r_2 + 0.885\delta r_1$, $r_2 + 1.77\delta r_1$ and amplitudes 1.0, 2.0, 1.0, 0.25, 1.0, 1.5, 1.0, 0.25, respectively. Two split Tl-Ba pairs are included in the fit with distances $r_3 - \delta r_3$, $r_3 + \delta r_3$. Three Tl-O pairs are also included.

The fit was started with the Tl displacement obtained from diffraction, 0.16 Å [10] (which corresponds to $\delta r_1 = 0.15$ Å and $\delta r_3 = 0.07$ Å). As was done for the fit to the $\langle 110 \rangle$ uncorrelated Tl displacement model, r_1 , r_2 , r_3 , and the amplitudes of the Tl and Ba peaks are fixed. The total number of variables is also 25. The quality of the constrained fit is about 30% worse than that of the fit for the $\langle 110 \rangle$ direction correlated displacement. The Tl-Tl peak at 3.87 Å is depressed by a large Debye-Waller factor, 0.2 Å, in the fitting process. The obtained distances, with $\delta r_1 = 0.25$ Å and $\delta r_3 = 0.06$ Å, deviate significantly from the starting model and are no longer consistent with the starting model. The extracted Tl-Tl PDF is plotted in Fig. 11d (solid line), which clearly moves away from the starting Tl-Tl PDF suggested by diffraction and towards the correlated Tl-Tl PDF (solid line in Fig. 11a).

The extracted Tl-Ba PDF is somewhat similar to that obtained from the $\langle 110 \rangle$ direction displacement, but it is difficult to distinguish between one broad peak, two split peaks, and three split peaks.

The above analyses clearly show that the Tl-Tl peak at the average lattice distance, 3.87 Å, is essentially destroyed by the large Debye-Waller factor in the uncorrelated Tl displacement model, for displacements along either the $\langle 110 \rangle$ or the $\langle 100 \rangle$ directions, and the extracted PPDF from the uncorrelated model tends to move away from the PPDF generated by the starting model and towards the PPDF obtained by the correlated model. Therefore, we conclude that our XAFS data do not support the uncorrelated Tl displacement along either the $\langle 110 \rangle$ direction or the $\langle 100 \rangle$ direction proposed by the diffraction studies [7,9,10]. We point out that XAFS is more sensitive than diffraction to small local structural distortions which have no long range order. This can be seen from the following example. Rietveld refinements were performed for Tl-2212 using 7 distorted models with different directions of displacement including two correlated PDF models [17]. The results of these refinements show relatively little sensitivity to the choice of model used for the TlO layers. Three models, *i.e.*, the uncorrelated four-fold displacement of both O(3) and Tl along the $\langle 100 \rangle$ directions, the uncorrelated four-fold displacement of O(3) along the $\langle 100 \rangle$ and Tl along the $\langle 110 \rangle$ directions, and the correlated two-fold displacement of both O(3) and Tl along the $\langle 110 \rangle$ directions (with the space group Pcca) [17], result in essentially the same quality of the fit to the data. In the XAFS data analysis, these three models can easily be distinguished as shown above. However, the model we proposed may not be unique. More complicated models may generate a similar PPDF to that shown in Fig. 11a.

B. Comparisons of XAFS data for samples with different T_c

The general picture presented in this paper for the distortions of the TlO layers is similar to that in Ref. 15, but with more extensive XAFS data for $Tl_2Ba_2CuO_y$ and more constraints on possible models. For the XAFS data at the Tl edge, both the Tl-Tl and Tl-Ba peaks are split into several peaks which all overlap; at the Ba edge, only the Ba-Tl peak is split. Therefore, the XAFS data analysis at the Tl edge is more complicated and technically involved than at the Ba edge. Although the Ba edge XAFS data are not quite as sensitive to the Tl distortion as the Tl edge XAFS data, they help rule out some possible models which fit the Tl edge XAFS data.

We also collected Tl L_{III} -edge XAFS data from another sample [12], $Tl_{1.85}Ba_2CuO_y$, with $T_c = 76$ K. This sample is made in a similar way as described in Sec. IIA. It has a tetragonal structure with lattice constants $a = 3.8626$ Å, $c = 23.224$ Å. We also have the Tl L_{III} -edge XAFS data used in the previous study [15], which were collected at 78 K from a tetragonal $Tl_2Ba_2CuO_y$ sample with $T_c = 89$ K and lattice constants $a = 3.866$ Å, $c = 23.239$ Å. All the data were reduced in exactly the same way as described in Sec. III.

The Tl L_{III} -edge XAFS data are plotted in Fig. 12 for the three samples with different T_c s; solid lines, $T_c = 60$ K; dotted lines, $T_c = 76$ K; dashed lines, $T_c = 89$ K. All the data can be fit with the model shown in Fig. 9. The difference

in the extracted distances from the constrained fit, among three samples, is within 0.01 \AA , although the amplitude of the Tl-O peak near 2 \AA varies significantly among the samples. This clearly shows that the local Tl displacement in the TlO layer is not sensitive to the structural symmetry and the transition temperature T_c . This local distortion is more likely intrinsic to the Tl-2201 compound, which will be further discussed in the following section.

There is a significant difference in the amplitude of the first peak at $r = 2.04 \text{ \AA}$ (*c*-axis Tl-O(2,3)). The amplitude was measured in two different ways. First, the amplitudes were obtained from the constrained fit using the FEFF5 standards, as described earlier assuming a single peak for the first Tl-O pair. Second, the data were fit one to another in the range of $1.0 \sim 1.8 \text{ \AA}$, and the relative amplitudes were obtained. The average amplitude is plotted in Fig. 13 as a function of T_c ; it is very close to a linear function. The higher the Tl-O amplitude of the peak near $r = 2 \text{ \AA}$, the lower T_c is. This trend is consistent with other experimental results [8,45,46]; a decrease in oxygen content of about $0.1 \sim 0.15$ per formula unit changed T_c from 0 to about $80 \sim 90 \text{ K}$ [45,46] although the absolute oxygen content was not well determined [8,45,46].

The data plotted in Fig. 13 are from three samples with different Tl and O contents which are not precisely determined. It has been reported that both the Tl and O contents can change T_c significantly [47]. The amplitude of the Tl-O peak plotted in Fig. 13 is from the contributions of the O(2) and the O(3) along the *c*-axis, and possibly an O(4) [8] if it exists. This amplitude can be affected in several ways: (a) a change in the O content at the O(2), O(3) and O(4) [8] sites, (b) the O movement between the O(3) and O(4) sites, (c) changes in the Tl-O(2) and Tl-O(3) (along the *c*-axis) distances, (d) a variation in the Tl content. From the limited data we have, it is not clear what is the main reason for the variation of the *measured* Tl-O amplitude which seems much too large to be explained solely by a variation in O content. However, Fig. 13 clearly shows that T_c is very sensitive to the O environment around the Tl atom. It is generally believed that the CuO_2 layer is the superconducting layer, thus this result also implies that a charge transfer occurs between the CuO_2 and TlO layers and it is mainly controlled by the O arrangement around the Tl, not the Cu substitution for Tl.

C. The Tl and Cu valences

The atomic valence (V) can be estimated from the obtained local structure using the Brown-Altermatt-Zachariasen formulae [48,49], which describe the relationship between the bond length (r) and the bond valence (s)

$$V = \sum s_i = \sum (r_i/r_o)^{-N} \quad (2)$$

or

$$V = \sum s_i = \sum \exp[(r_o - r_i)/B], \quad (3)$$

where r_o , N and B are empirically determined parameters [48,49]. For $\text{Tl}^{3+}\text{-O}$, we used Eq. (2) with the most recent available parameters, $r_o=2.04$ and $N=6.4$ [50] and the structural model (Fig. 9) constructed based on our XAFS results for the sample with the highest O concentration. The calculated Tl valence is $(2.95 \pm 0.05)_+$, very close to the formal valence, $3+$ ($\text{Tl}_2^{3+}\text{Ba}_2^{2+}\text{Cu}^{2+}\text{O}_6^{2-}$). This is also consistent with the photoemission [51,52] and the x-ray-absorption near-edge spectra [15] measurements which indicate a Tl valence slightly less than $3+$. If both the Tl and O(3) atoms were at their ideal sites ($4e$), the calculated effective valence for Tl would be $2.77+$, which is too small compared to the formal valence and not stable for the Tl ion (the Tl ion should be either Tl^{1+} or Tl^{3+}). This is probably part of the reason why the TlO layer is distorted.

We also calculated the Cu valence, using Eq. (3) with $B = 0.37$, $r_o = 1.679 \text{ \AA}$ [49] and the local structure derived from XAFS (Table I). The calculated Cu valence is $(2.15 \pm 0.05)_+$, which is very close to the Cu(2) valence in $\text{YBa}_2\text{Cu}_3\text{O}_7$ ($2.20+$) [53–55] and Cu in $\text{Tl}_2\text{Ba}_2\text{CaCu}_2\text{O}_8$ ($2.11+$) [56] calculated using the same formula. Our estimated effective valences for Cu and Tl are qualitatively in agreement with the charge transfer (or local charge) picture between the TlO and CuO_2 layers [54], *i.e.*, $\text{Tl}_2\text{O}_3 + \text{CuO} \rightarrow [\text{Tl}_2\text{O}_3]^{\delta-} + [\text{CuO}]^{\delta+}$. It is generally believed that the extra holes in the CuO_2 are predominantly at the O site [57–59]. However, it is not clear where the extra

electrons are in the TlO layers. We note that the extra holes in the CuO₂ layer are not solely introduced by the reduction of the Tl valence. The variation in O content can also change the hole concentration in the CuO₂ layer. A decrease in O content of about 0.1 per formula unit, which corresponds to a decrease in hole concentration of 0.2, increases T_c from ~0 to ~90 K [45,46]. However, there is a controversy in the literature about the absolute, optimum O content for samples with the highest T_c [11,12,45,46].

D. The question of long range order

Long range order modulations have been observed in Bi-Sr-Ca-Cu-O superconductors and related materials [43]. Some long range order in the TlO layers is also observed in Tl-2201 and Tl-2212 by electron diffraction and high-resolution transmission electron microscopy [18–22]. The modulation wave vector is about $\langle -0.16, 0.08, 1 \rangle$ for tetragonal Tl-2201 ($a = b \simeq 3.8 \text{ \AA}$), $\langle 0.08, 0.24, 1 \rangle$ for orthorhombic Tl-2201 ($a \simeq b \simeq 5.4 \text{ \AA}$), and $\langle 0.17, 0, 1 \rangle$ for tetragonal Tl-2212. The superlattice for the first case would have a large unit cell, $6a \times 12b$ in the ab-plane. However, these superlattices [18,21] are usually observed only with selected-area electron diffraction and are much weaker in intensity than in the Bi-Sr-Ca-Cu-O superconductors which exhibit strong supercell diffraction structure [43] and c-axis displacements in the TlO layers are small (see Sec. VI.A). Such superstructures are not always observed in the tetragonal Tl-2201 samples [22]. Consequently, this long range order of the lattice distortions in the Tl-based superconductors seems weak, sample dependent, and may not be intrinsic. Since both the Tl and O(3) atoms can be shifted in two equivalent directions in the model we have proposed, material with this distorted local structure might well have a superstructure over a limited range, which is qualitatively consistent with the above electron diffraction measurements. There are many ways to construct superstructures with periodicity of $6a \times 12b$ using the distorted $2a \times 2b$ unit cell shown in Fig. 9 for the TlO layers. Two possible examples that are probably over simplified are shown in Fig. 14. Here the Tl displacements (not shown) are the same from one $2a \times 2b$ cell to another, but the direction of the O displacements varies. In the upper panel, the O positions are not periodic; some O atoms move together or apart, while others move in the same direction. In the lower panel, the direction of the O displacements is rotated by 90° in the right half of the supercell.

VII. CONCLUSIONS

The local structure of Tl₂Ba₂CuO_y, with an orthorhombic phase and T_c=60 K, has been studied at the Cu K-, Ba K-, and Tl L_{III}-edges using the XAFS technique. Several new approaches have been implemented, *e.g.*, direct structural simulations up to 7 Å using the FEFF5 code, constrained fits, and comparisons of PPDFs for different models.

Both the qualitative and quantitative data analyses clearly show that the Cu, O(1), O(2), and Ba atoms are at their ideal sites in the unit cell as given by the diffraction studies, while the Tl and O(3) atoms are displaced from the sites suggested by the average crystal structure. The Tl-Tl distance at $r=3.5 \text{ \AA}$ between the TlO layers remains, but the Tl-Tl distance at 3.9 \AA in the TlO layer is not observed and the Tl-Ba and Ba-Tl peaks are very broad. The shorter Tl-O(3) distance in the TlO layer is about 2.33 \AA , significantly shorter than the distance calculated with both the Tl and O(3) atoms at their ideal $4e$ sites ($x = y = 0$ or $\frac{1}{2}$). An excellent fit to the XAFS data can be achieved with a correlated displacement model shown in Fig. 9. The fitting results show that the Tl atom is displaced along the $\langle 110 \rangle$ direction from its ideal site by about 0.11 \AA and the O(3) atom is shifted from the $4e$ site by about 0.53 \AA roughly along the $\langle 100 \rangle$ direction. This model also fits very well to the XAFS data collected from two tetragonal Tl₂Ba₂CuO_y samples with different T_cs.

The XAFS data do not support the uncorrelated displacement models proposed by diffraction investigations [7,9,10]. Our model is similar to that proposed by the PDF analyses of the neutron scattering data on Tl-2212 [16], but is more specific about the relative shift of the Tl atoms between the two consecutive TlO layers. However, the Tl displacement, 0.11 \AA , obtained in our study, is only one third of the value (0.32 \AA) suggested by the PDF.

The estimated Cu and Tl valences imply a charge transfer between the CuO_2 and TlO layers which is consistent with other experimental results [15,42,51,52]. The estimated Tl valence also supports the distorted structure of the TlO layer obtained from our XAFS analysis. The estimated Tl valence (2.95+) in the distorted TlO layer is much closer to its formal valence (3+) than that (2.77+) estimated from the ideal TlO layer.

A comparison of the XAFS data at the Tl L_{III} - edge from three $\text{Tl}_2\text{Ba}_2\text{CuO}_y$ samples clearly shows a correlation between the transition temperature and the local O environment around the Tl atoms. This implies that the hole concentration in the CuO_2 layer is mainly controlled by the O arrangement about the Tl in those samples, and not by Cu substitution for the Tl.

ACKNOWLEDGMENTS

We thank Corwin Booth for help in the data collection. The experiments were performed at the Stanford Synchrotron Radiation Laboratory, which is operated by the U.S. Department of Energy, Division of Chemical Sciences, and by the NIH, Biomedical Resource Technology Program, Division of Research Resources. The experiment is partially carried out on UC/National Laboratories PRT beam time. The work is supported in part by NSF grant DMR-92-05204.

-
- [1] B. K. Agrawal, S. Kumar, S. Agrawal, and P. S. Yadav, *Phys. Rev. B* **48**, 7364 (1993).
 - [2] R. V. Kasowski, W. Y. Hsu, and F. Herman, *Phys. Rev. B* **38**, 6470 (1988).
 - [3] Z. Z. Sheng and A. M. Hermann, *Nature* **332**, 55 (1988).
 - [4] C. C. Torardi, M. A. Subramanian, J. C. Calabrese, J. Gopalakrishnan, E. M. McCarron, K. J. Morrissey, T. R. Askew, R. B. Flippen, U. Chowdhry, and A. W. Sleight, *Phys. Rev. B* **38**, 225 (1988).
 - [5] J. B. Parise, J. Gopalakrishnan, M. A. Subramanian, and A. W. Sleight, *J. Solid State Chem.* **76**, 432 (1988).
 - [6] A. W. Hewat, P. Bordet, J. J. Capponi, C. Chaillout, J. Chenavas, M. Godinho, E. A. Hewat, J. L. Hodeau, and M. Marezio, *Physica C* **156**, 369 (1988).
 - [7] J. B. Parise, C. C. Torardi, M. A. Subramanian, J. Gopalakrishnan, A. W. Sleight, E. Prince, *Physica C* **159**, 239 (1989).
 - [8] Y. Shimakawa, Y. Kubo, T. Manako, H. Igarashi, F. Izumi, and Asano, *Phys. Rev. B* **42**, 10165 (1990).
 - [9] N. N. Kolesnikov, V. E. Korotkov, M. P. Kulakov, R. P. Shibaeva, V. N. Molchanov, R. A. Tamazyan, and V. I. Simonov, *Physica C* **195**, 219 (1992).
 - [10] R. S. Liu, S. D. Hughes, R. J. Angel, T. P. Hackwell, A. P. Mackenzie, and P. P. Edwards, *Physica C* **198**, 203 (1992).
 - [11] T. Manako, Y. Kubo, and Y. Shimakawa, *Phys. Rev. B* **46**, 11019 (1992).
 - [12] C. Ström, S.-G. Eriksson, A. Simon, Hj. Mattausch and P. K. Kremer, accepted for publication in *J. Solid State Chem.*
 - [13] Y. Shimakawa, *Physica C* **204**, 247 (1993).
 - [14] C. Ström, Ph.D thesis, University of Göteborg (1993).
 - [15] G. G. Li, J. Mustre de Leon, S. D. Conradson, M. V. Lovato, and M. A. Subramanian, *Phys. Rev. B*, to be published.

- [16] W. Dmowski, B. H. Toby, T. Egami, M. A. Subramanian, J. Gopalakrishnan, and A. W. Sleight, *Phys. Rev. Lett.* **61**, 2608 (1988).
- [17] B. H. Toby, W. Dmowski, T. Egami, J. D. Jorgensen, M. A. Subramanian, J. Gopalakrishnan, and A. W. Sleight, in *High Temperature Superconductors: Relationships Between Properties, Structure, and Solid-State Chemistry*, edited by J. D. Jorgensen *et al* (Materials Research Society, Pittsburgh, Pennsylvania, 1989), p.309.
- [18] S. S. P. Parkin, V. Y. Lee, A. I. Nazzal, R. Savoy, T. C. Huang, G. Gorman, and R. Beyers, *Phys. Rev.* **B 38**, 6531 (1988).
- [19] J. D. Fitz Gerald, R. L. Withers, J. G. Thompson, L. R. Wallenberg, J. S. Anderson, and B. G. Hyde, *Phys. Rev. Lett.* **60**, 2797 (1988).
- [20] T. Oku, K. Hiraga, D. Shindo, M. Kukuchi, S. Nakajima, and Y. Syono, in *Advances in Superconductivity III*, edited by K. Kajimura and H. Hayakawa (Springer-Verlag, New York, 1990), p. 367.
- [21] R. Beyers, S. S. Parkin, V. Y. Lee, A. I. Nazzal, R. Savoy, G. Gorman, T. C. Huang, and S. La Placa, *Appl. Phys. Lett.* **53**, 432 (1988).
- [22] S. Nakajima, T. Oku, R. Suzuki, M. Kikuchi, K. Hiraga, and Y. Syono, *Physica C* **214**, 80 (1993).
- [23] J. Mustre de Leon, G. G. Li, S. D. Conradson, A. R. Bishop, M. A. Subramanian, I. D. Raistrick, *Physica C* **220**, 377 (1994).
- [24] H. Yamaguchi, S. Nakajima, Y. Kuwahara, H. Oyanagi, and Y. Syono, *Physica C* **213**, 375 (1993).
- [25] B. H. Toby, T. Egami, J. D. Jorgensen and M. A. Subramanian, *Phys. Rev. Lett.* **64**, 2414 (1990).
- [26] P. G. Allen, J. Mustre de Leon, S. D. Conradson, and A. R. Bishop, *Phys. Rev. B* **44**, 9480 (1991).
- [27] T. M. Hayes and J. B. Boyce in *Solid State Physics*, edited by H. Ehrenreich, F. Seitz, and D. Turnbull (Academic, New York, 1982), Vol. **37**, p.173.
- [28] E. A. Stern and S. M. Heald, in *Handbook on Synchrotron Radiation*, edited by E. E. Koch (North-Holland, New York, 1983), Vol. 1, p. 955.
- [29] G. G. Li, F. Bridges, J. B. Boyce, and W. C. H. Joiner, *Phys. Rev. B* **47**, 12110 (1993).
- [30] F. Bridges, G. G. Li and Xun Wang, *Nucl. Instr. and Meth. A* **320**, 548 (1992); G. G. Li, F. Bridges, and X. Wang, *ibid*, **340**, 420 (1994).
- [31] J. J. Rehr, J. Mustre de Leon, S. Zabinsky, and R. C. Albers, *J. Chem. Soc.* **113**, 5135 (1991); J. Mustre de Leon, J. J. Rehr, S. I. Zabinsky, and R. C. Albers, *Phys. Rev. B* **44**, 4146 (1991).
- [32] G. G. Li, F. Bridges, unpublished.
- [33] G. G. Li, F. Bridges, and G. S. Brown, *Phys. Rev. Lett.* **68**, 1609 (1992).
- [34] C. H. Booth, F. Bridges, J. B. Boyce, T. Claeson, Z. X. Zhao, and P. Cervantes, *Phys. Rev. B* **49**, 3432 (1994).
- [35] J. J. Rehr, C. H. Booth, F. Bridges, and S. I. Zabinsky, *Phys. Rev. Lett.* **xx**, to be published.
- [36] A. I. Frenkel, E. A. Stern, M. Qian, and M. Neville, *Phys. Rev.* **B 48**, 12449 (1993).
- [37] A. Filipponi, L. Ottaviano, and T. A. Tyson, *Phys. Rev.* **A 48**, 2098 (1993).
- [38] P. D'Angelo, A. Di Cicco, A. Filipponi, and N. V. Pavel, *Phys. Rev.* **A 47**, 2055 (1993).
- [39] E. A. Stern, *Phys. Rev.* **B 48**, 9825 (1993).
- [40] F. Bridges, J. B. Boyce, T. Claeson, T. H. Geballe, and J. M. Tarascon, *Phys. Rev. B* **39**, 11603(1989).

- [41] J. B. Boyce, F. Bridges, T. Claeson, and M. Nygren, Phys. Rev. B **39**, 6555(1989).
- [42] G. G. Li, J. Mustre de Leon, S. D. Conradson, M. V. Lovato, and M. A. Subramanian, Physica C **219**, 371 (1994).
- [43] J. M. Tarascon, W. R. McKinnon, and Y. LePage, in *Chemistry of High Temperature Superconductors*, edited by C. N. R. Rao (World Scientific, New Jersey, 1991), p. 186.
- [44] In this paper, we have used $S_o^2=0.9$ for the Tl-Tl pair. In Ref. 9, S_o^2 was set to be about 0.5 which seems too small according to our recent detailed comparison of FEFF5 calculation with experimental XAFS [32].
- [45] Y. Shimakawa, Y. Kubo, T. Manako, T. Satoh, S. Iijima, T. Ichihashi, and H. Igarashi, Physica C **157**, 279 (1989).
- [46] M. Kikuchi, S. Nakajima, Y. Syono, K. Nagase, R. Suzuki, T. Kajitani, N. Kobayashi, and Y. Muto, Physica C **166**, 497 (1990).
- [47] K. K. Saini, C. P. Sharma, Chanderkant, D. K. Suri, K. B. Ravat, Subhas Chandra, and S. P. Tewari, Physica C **216**, 59 (1993).
- [48] I. D. Brown, in *Structure and Bonding in Crystals*, edited by M. O’Keeffe and A. Navrotsky (Academic Press, New York, 1981), Vol. II, p.1.
- [49] I. D. Brown and D. Altermatt, Acta Cryst. **B41**, 244 (1985).
- [50] H. H. Otto, R. Baltrusch, and H.-J. Brandt, Physica C **215**, 205 (1993).
- [51] S. Nakajima *et al*, Physica C **160**, 458 (1989).
- [52] T. Suzuki *et al*, Physica C **162-164**, 1387 (1989); T. Suzuki *et al*, Phys. Rev. B **40**, 5184 (1989).
- [53] I. D. Brown, J. Solid State Chem. **82**, 122 (1989).
- [54] R. J. Cava, Science **247**, 656 (1990).
- [55] R. J. Cava *et al*, Physica C **165**, 419 (1990).
- [56] A. W. Hewat, E. A. Hewat, J. Brynestad, H. A. Mook, and E. D. Specht, Physica C **152**, 438 (1988).
- [57] H. Romberg *et al*, Phys. Rev. B **41**, 2609 (1990).
- [58] J. C. Fuggle *et al*, Phys. Rev. B **37**, 123 (1988).
- [59] V. J. Emery, Phys. Rev. Lett. **58**, 2794 (1987).

FIG. 1. The crystal structure for $Tl_2Ba_2CuO_y$ showing the definitions for the different O sites. Half of the unit cell is shown and the whole unit cell is symmetric about the CuO_2 plane. The dotted lines indicate the atomic positions in the half unit cell. The structural parameters used here are from Ref. 4, in which the O(3) atom is displaced from the 4e site along the a-axis by 0.37 Å.

FIG. 2. The k-space XAFS data at the Cu K-, Ba K-, and Tl L_{III} -edges in $Tl_2Ba_2CuO_y$.

FIG. 3. (a-b) The absorptance above the Ba K-edge (a) and the Tl L_{III} -edge (b) in $Tl_2Ba_2CuO_y$; solid lines, experimental data; dotted lines, fits to the data using cubic splines; dashed lines, fits to the data using cubic splines plus the extracted background from BaO and Tl_2O_3 , respectively. The dotted lines and dashed lines are used to simulate the “free-atom absorptance”. (c-d) The Fourier transform of the Ba K-edge (c) and the Tl L_{III} -edge (d) XAFS data from $Tl_2Ba_2CuO_y$, using the “free-atom absorptance” obtained from cubic spline fits (dotted line) and cubic spline plus corresponding extracted background fits (solid lines), respectively. The transform ranges are over 3.5 to 15.5 \AA^{-1} at the Ba edge and 3.3 to 15.5 \AA^{-1} at the Tl edge, and both are Gaussian broadened by 0.3 \AA^{-1} . The fast oscillatory curves are the real parts of the complex transforms and the envelope curves are the magnitudes of the transforms.

FIG. 4. The Fourier transform of the Cu K-edge XAFS, $k\chi(k)$, to real space for $Tl_2Ba_2CuO_y$. The transform range is over 3.1 to 16.5 \AA^{-1} , Gaussian broadened by 0.3 \AA^{-1} . The fast oscillatory curve is the real part of the complex transform and the envelope curve is the magnitude of the transform. The solid lines are the experimental data and the dotted lines are the *simulations* (without a fit) using the FEFF5 code with the average crystallographic structure [4] including all the pairs within 7.5 \AA .

FIG. 5. The Fourier transform of the Ba K-edge XAFS, $k\chi(k)$, to real space for $Tl_2Ba_2CuO_y$. The transform range is over 3.5 to 15.5 \AA^{-1} , Gaussian broadened by 0.3 \AA^{-1} . The fast oscillatory curve is the real part of the complex transform and the envelope curve is the magnitude of the transform. The solid lines are the experimental data and the dotted lines are the *simulations* using the FEFF5 code, (a) with the average crystallographic structure [4], and (b) with the local distorted structural model (Fig. 9), including all the pairs within 7.5 \AA . Part (c) shows a small section of the x -axis enlarged: experimental data (solid lines), simulations from part (a) (dotted lines), and simulations from part (b) (dots).

FIG. 6. The Fourier transform of the Tl L_{III} -edge XAFS, $k\chi(k)$, to real space for $Tl_2Ba_2CuO_y$. The transform range is over 3.3 to 15.5 \AA^{-1} , Gaussian broadened by 0.3 \AA^{-1} . The fast oscillatory curve is the real part of the complex transform and the envelope curve is the magnitude of the transform. The solid lines are the experimental data and the dotted lines are the *simulations* using the FEFF5 code, (a) with the average crystallographic structure [4], and (b) with the local distorted structural model (Fig. 9), including all the pairs within 7.5 \AA . Note that no fit of the simulated XAFS to the experimental data has been made (for more information, see text).

FIG. 7. The Fourier transform of $k\chi(k)$ at the Cu K-edge for $Tl_2Ba_2CuO_y$. The transform range is the same as in Fig. 4. Both the real part and the magnitude of the transform are plotted. The solid lines are the experimental data and the dotted lines are the fits to the data. The fitting range is 1.0 to 3.9 \AA .

FIG. 8. The Fourier transform of $k\chi(k)$ at the Ba K-edge for $Tl_2Ba_2CuO_y$. The transform range is the same as in Fig. 5. Both the real part and the magnitude of the transform are plotted. (a) The comparison between the experimental curves and fits to the data. The fitting range is 1.2 to 3.8 \AA . The solid lines are the experimental data and the dotted lines are the fits. (b) The contributions of the Ba-O, -Cu, and -Ba peaks in the fit. (c) The contributions of the Ba-Tl pairs. The top trace is the sum of the Ba-Tl peaks, followed by the three individual peaks.

FIG. 9. The projection of the local structural model in the ab -plane for the distorted TlO layers. Two successive layers are shown. The best overall agreement between the model and the XAFS results is achieved when the Tl atom is shifted along the $\langle 110 \rangle$ direction by 0.11 \AA and the O atom in the TlO layer is shifted along the $[100]$ and/or $[010]$ directions by about 0.53 \AA from its ideal site. The O displacement along the $[010]$ direction is not shown in the figure. Note that the displacements of the Tl and O atoms are *correlated*, not random.

FIG. 10. The Fourier transform of $k\chi(k)$ at the Tl L_{III} -edge for $Tl_2Ba_2CuO_y$. The transform range is the same as in Fig. 6. Both the real part and the magnitude of the transform are plotted. (a) The comparison between the experiment results and fits to the data. The fitting range is 1.2 to 4.2 Å. The solid lines are the experimental data and the dotted lines are the fits to the data. (b) The contributions of the Tl-O peaks in the fit. (c) The contributions of the Tl-Tl pairs. The top trace is the sum of the Tl-Tl peaks, followed by the three individual peaks. (d) The contributions of the Tl-Ba pairs. The top trace is the sum of the Tl-Ba peaks, followed by the three individual peaks.

FIG. 11. The Tl-Tl pair-distribution-function (PDF) from (a) the correlated Tl displacement model (refer to Fig. 9), (b) the ideal structure, (c) the uncorrelated Tl displacements along the $\langle 110 \rangle$ direction, and (d) the uncorrelated Tl displacements along the $\langle 100 \rangle$ direction. The dotted lines are the starting PDFs and solids are the extracted Tl-Tl PDFs from XAFS using the corresponding structural models and the constrained fits. For more information, see Sec. VI.A.

FIG. 12. The Fourier transform of the Tl L_{III} -edge XAFS, $k\chi(k)$, to real space. The transform range is over 3.2 to 15.5 Å⁻¹, Gaussian broadened by 0.3 Å⁻¹. Both the real part and the magnitude of the Fourier transform are plotted. The data are collected at $T=80\pm 2$ K from three samples with $T_c=60$ K (orthorhombic, solid lines), $T_c=76$ K (tetragonal, dotted lines), and $T_c=89$ K (tetragonal, dashed lines), respectively. For more information, refer to Sec. VI.B.

FIG. 13. The amplitude of the nearest Tl-O peak near $r = 2$ Å versus T_c for three samples presented in Fig. 12.

FIG. 14. Two possible models for the $6a \times 12b$ superlattice. The Tl displacements are the same from one $2a \times 2b$ unit cell to another while the O displacements vary.

TABLE I. Cu local structure obtained from XAFS and diffraction. “nbrs” indicates the weighted number of neighbors. The estimated errors are: number of neighbors, $\pm 15\%$; distances, $\pm 0.02 \text{ \AA}$.

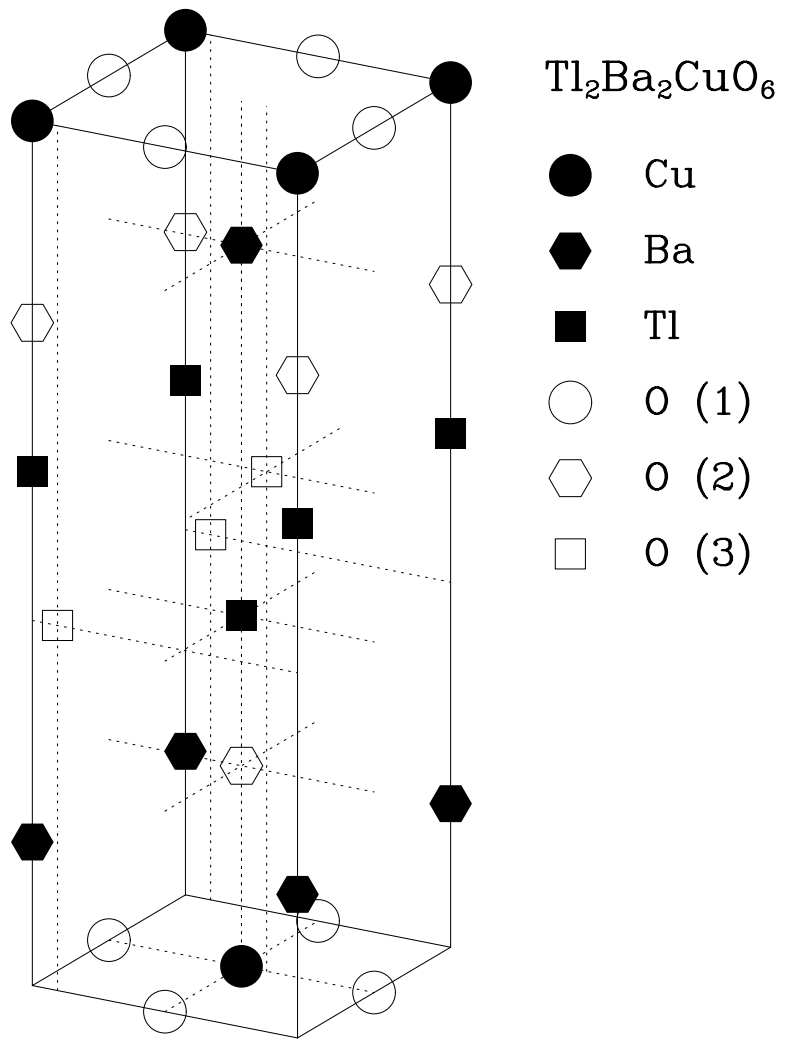
Pairs	XAFS			Diffraction	
	$r(\text{\AA})$	nbrs	$\sigma(\text{\AA})$	$r(\text{\AA})$	nbrs
Cu-O(1)	1.93	3.8	0.038	1.93	4
Cu-O(2)	2.71	1.9	0.093	2.72	2
Cu-Ba	3.35	7.7	0.053	3.35	8
Cu-Cu	3.86	3.2	0.046	3.87	4
Cu-O(1)	4.31	7.7	0.056	4.32	8

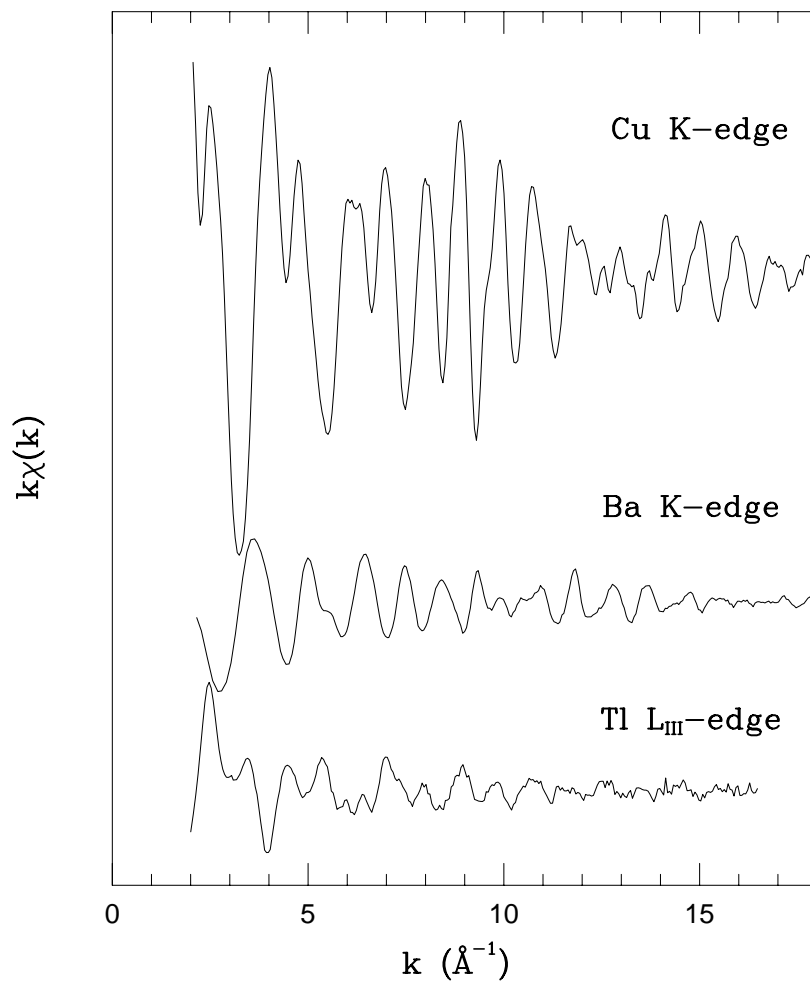
TABLE II. Ba local structure from XAFS, diffraction, and the model. The values listed in the brackets are from other diffraction studies [4–11]. “nbrs” indicates the weighted number of neighbors. In the model, the Tl atoms are shifted from the 4e site along the $\langle 110 \rangle$ direction by 0.11 \AA and the O(3) atoms are shifted from the 4e site by 0.53 \AA along the $\langle 100 \rangle$ direction. The estimated errors are: number of neighbors, $\pm 15\%$; distances, $\pm 0.02 \text{ \AA}$.

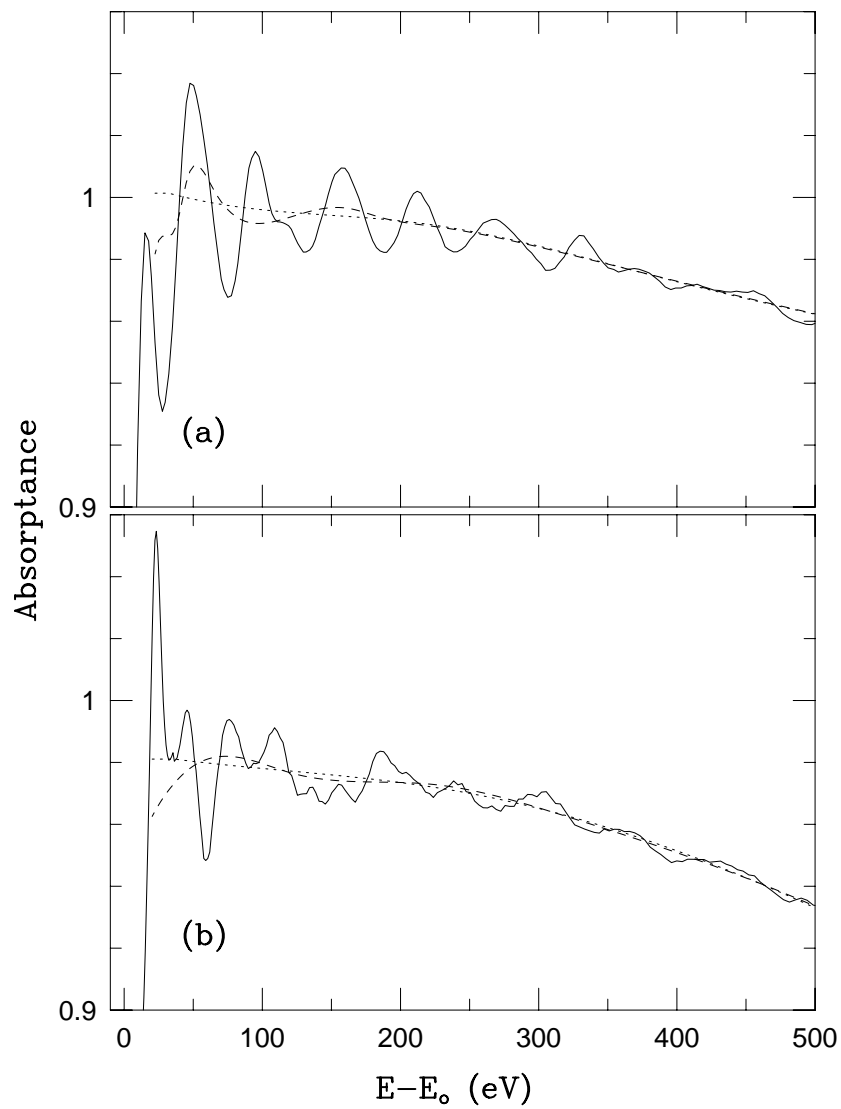
Pairs	XAFS			Diffraction		Model	
	$r(\text{\AA})$	nbrs	$\sigma(\text{\AA})$	$r(\text{\AA})$	nbrs	$r(\text{\AA})$	nbrs
Ba-O(1)	2.73	4.0	0.046	2.74	4		
Ba-O(2)	2.83	4.0	0.054	2.84	4		
Ba-O(3)	2.97	1.0	0.040	2.95 (2.95-3.00)	1	2.98	1
Ba-Cu	3.35	4.1	0.053	3.35	4		
Ba-Ba	3.87	6.0	0.066	3.87	5		
Ba-Tl	3.80	1.0	0.060	3.89	4	3.81	1
	3.90	2.0	0.060			3.89	2
	4.00	1.0	0.060			3.97	1

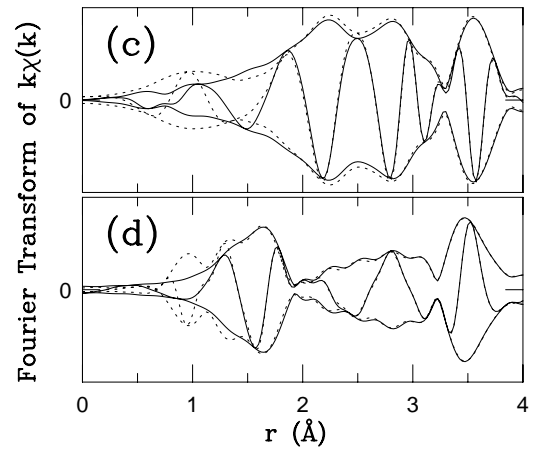
TABLE III. Tl local structure obtained from XAFS, diffraction, and the model. The values listed in the brackets are from other diffraction studies [4–11]. “nbrs” indicates the weighted number of neighbors. In the model, the Tl atoms are shifted from the 4e site along the $\langle 110 \rangle$ direction by 0.11 \AA and the O(3) atoms are shifted from the 4e site by 0.53 \AA along the $\langle 100 \rangle$ direction. The estimated errors are: number of neighbors, $\pm 15\%$; distances, $\pm 0.02 \text{ \AA}$.

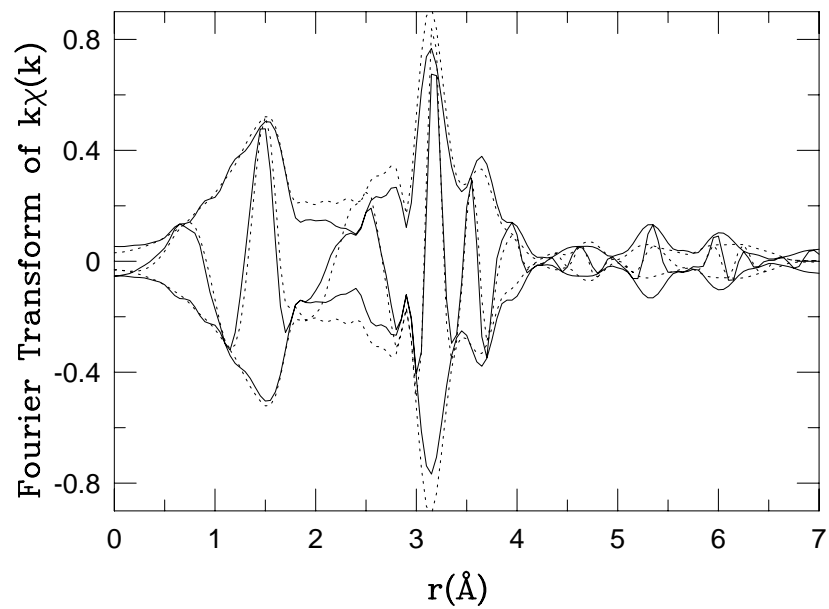
Pairs	XAFS			Diffraction		Model	
	$r(\text{\AA})$	nbrs	$\sigma(\text{\AA})$	$r(\text{\AA})$	nbrs	$r(\text{\AA})$	nbrs
Tl-O(2,3)	2.04	1.8	0.045	1.99 (1.98-2.01)	1	2.00	1
				2.05 (2.01-2.09)	1	2.09	1
Tl-O(3)	2.33	(2.6)	0.131	2.43-3.07 (2.31-3.22)	4	2.29-2.38	2
						3.12-3.24	2
Tl-O(2)	4.39	5.4	0.117	4.35	6	4.28-4.44	6
Tl-Tl	3.51	4.2	0.081	3.51	4	3.51	2
						3.52	2
	3.72	2.1	0.069	3.87	4	3.72	2
	4.03	2.1	0.114			4.02	2
Tl-Ba	3.82	0.95	0.060	3.89	4	3.81	1
	3.90	1.9	0.060			3.89	2
	3.98	0.95	0.060			3.97	1

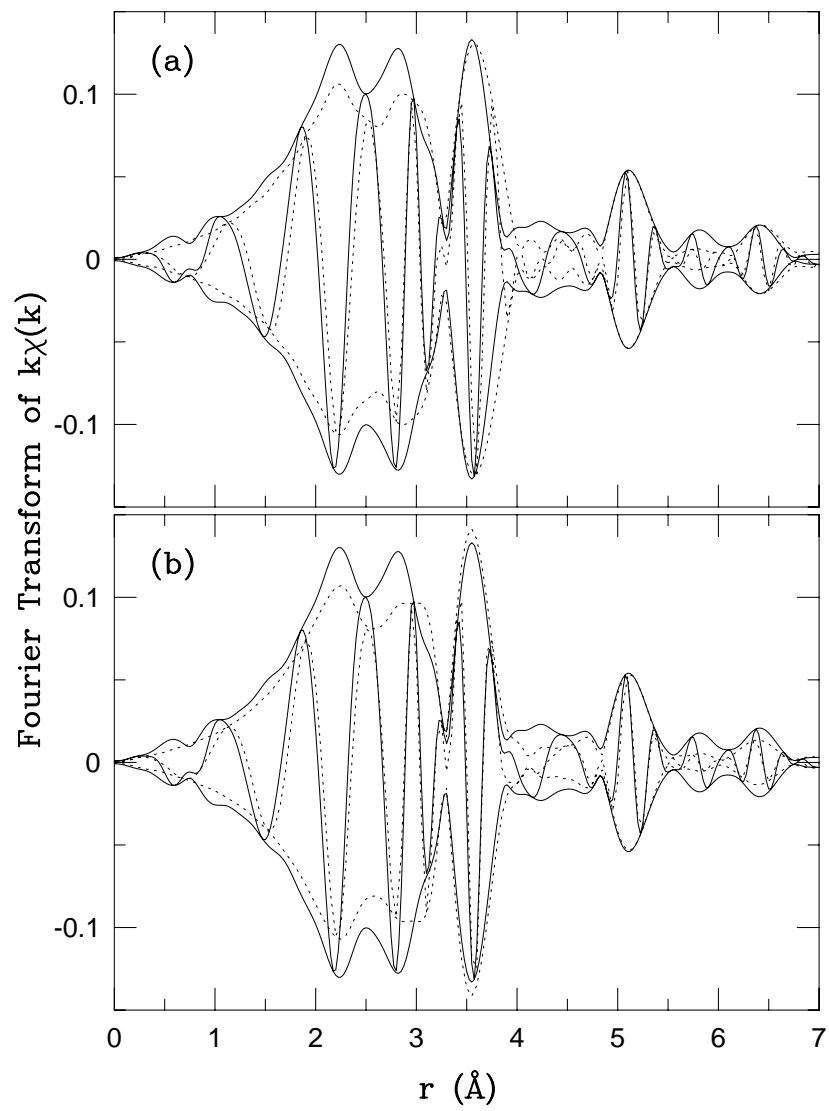


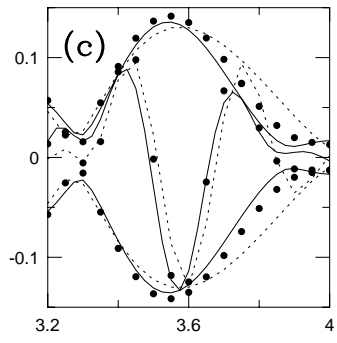


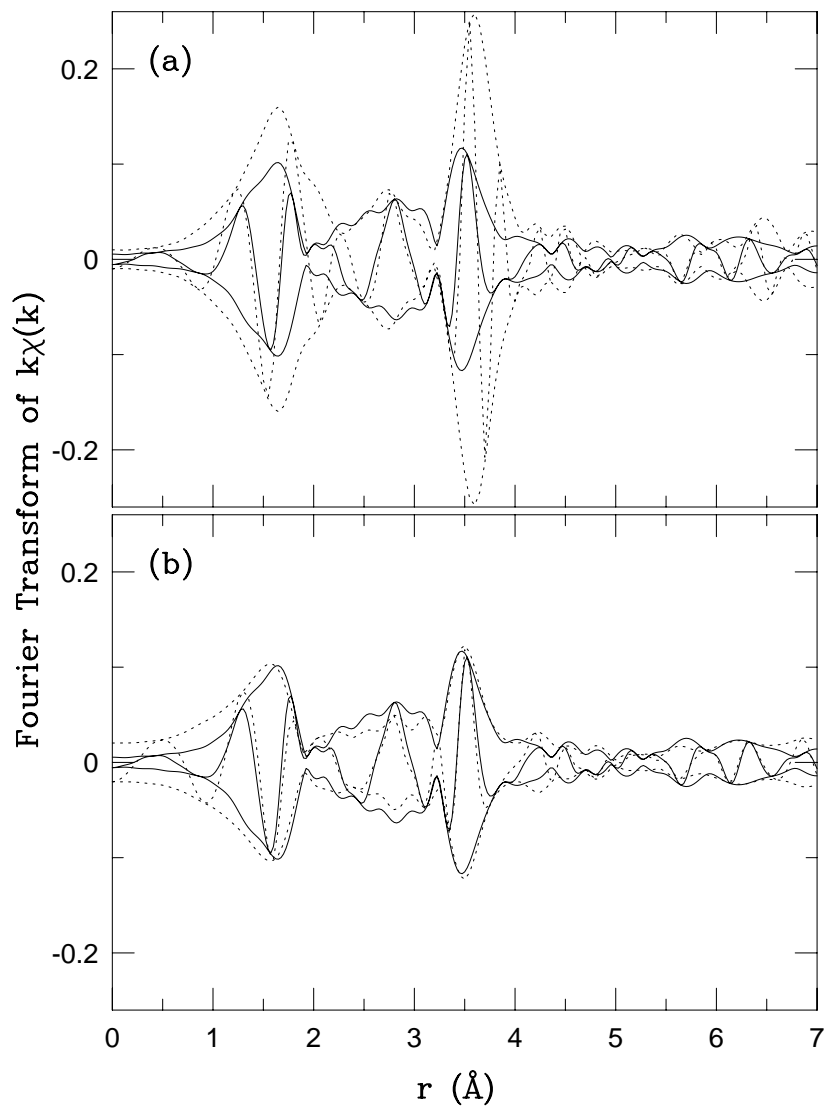


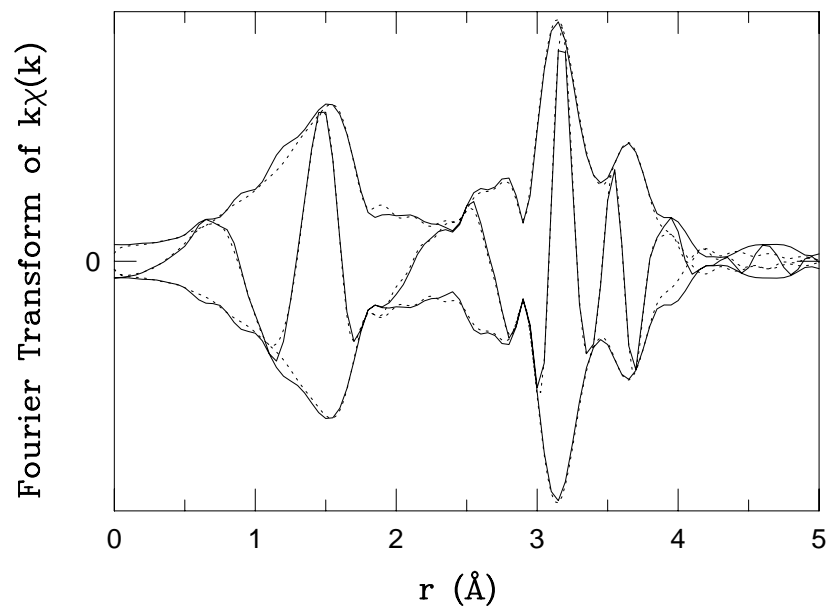


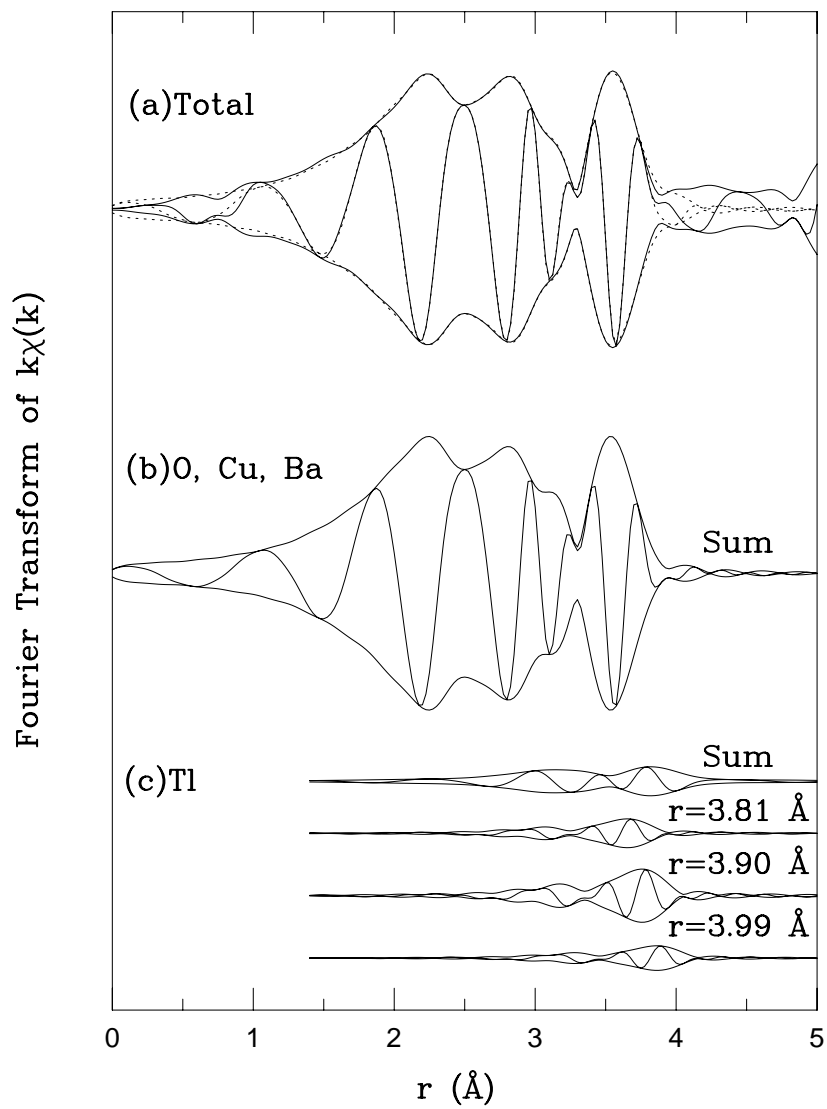


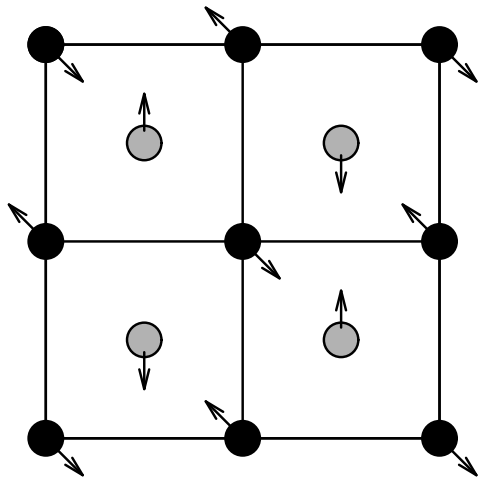








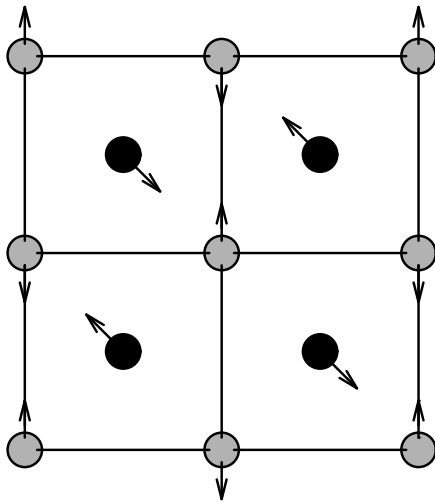




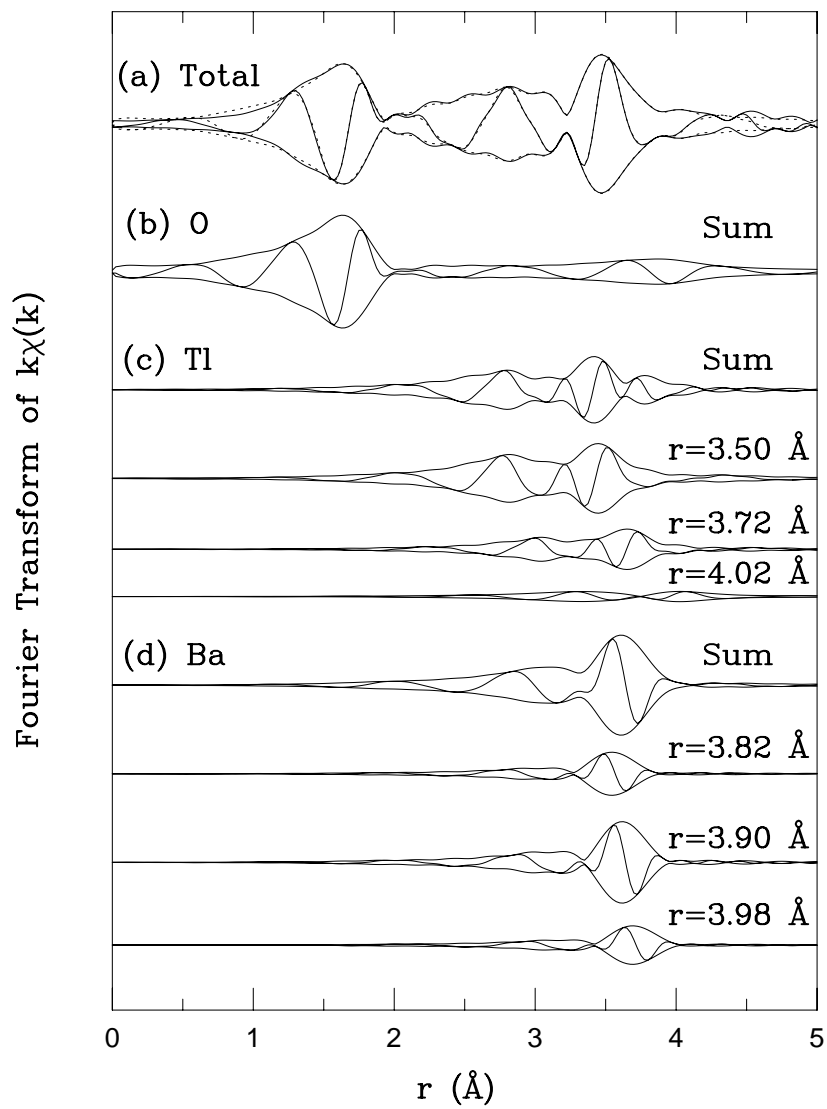
First TiO layer

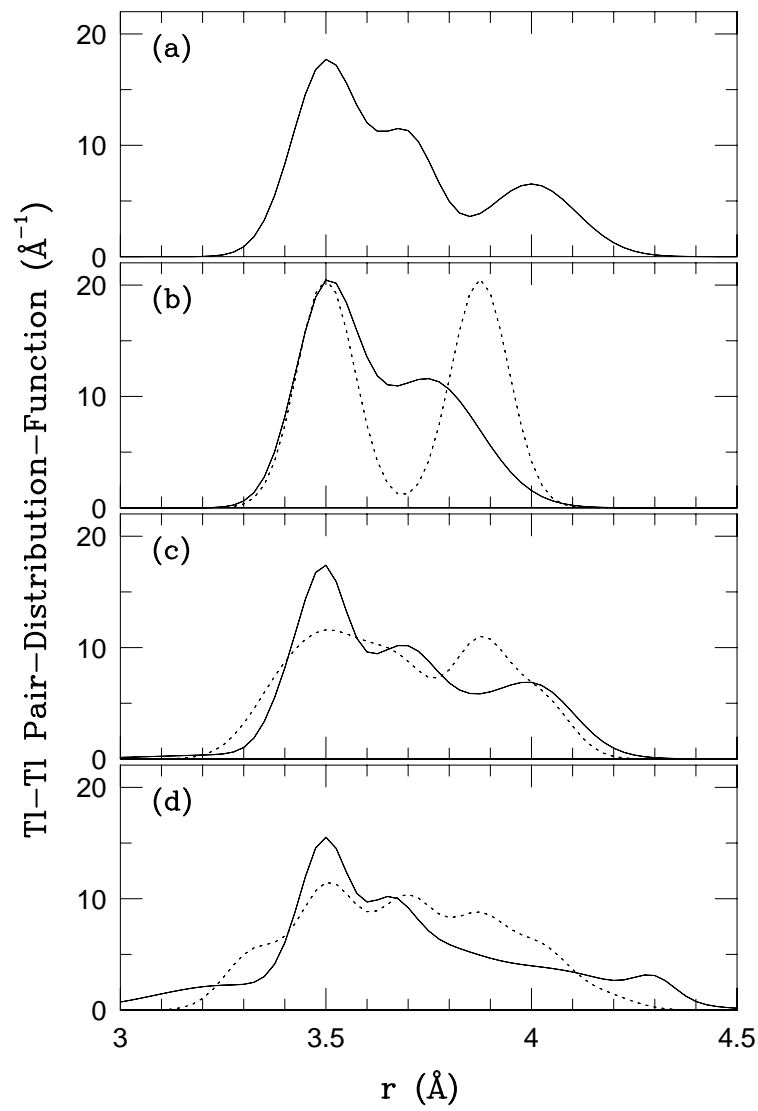
● Ti atom

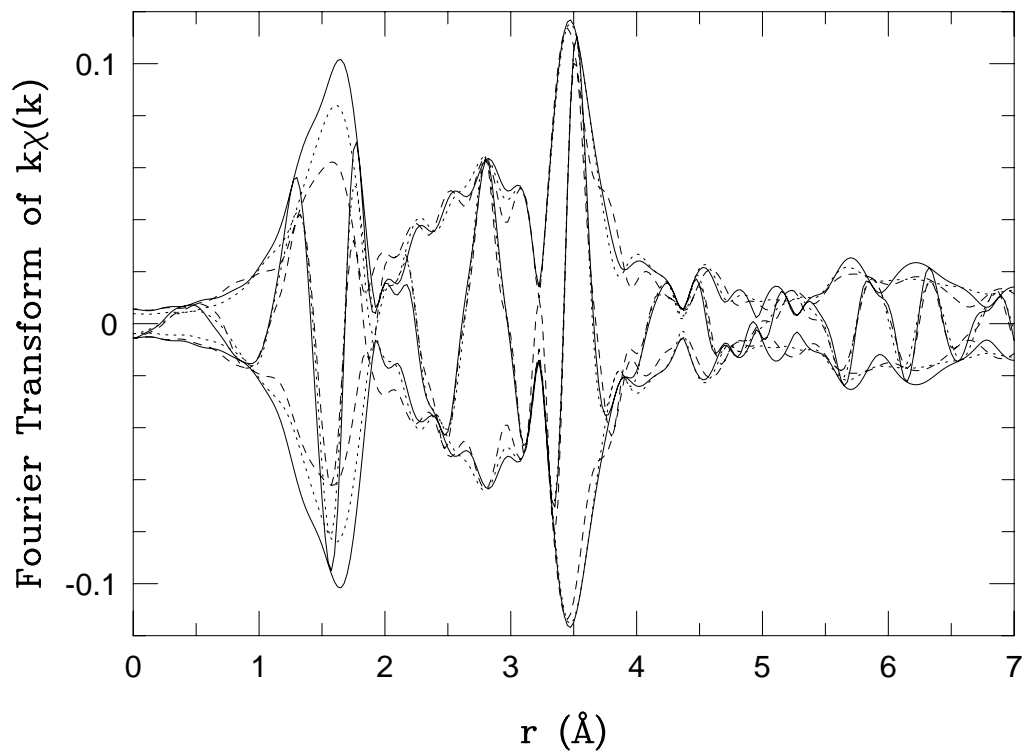
○ O atom

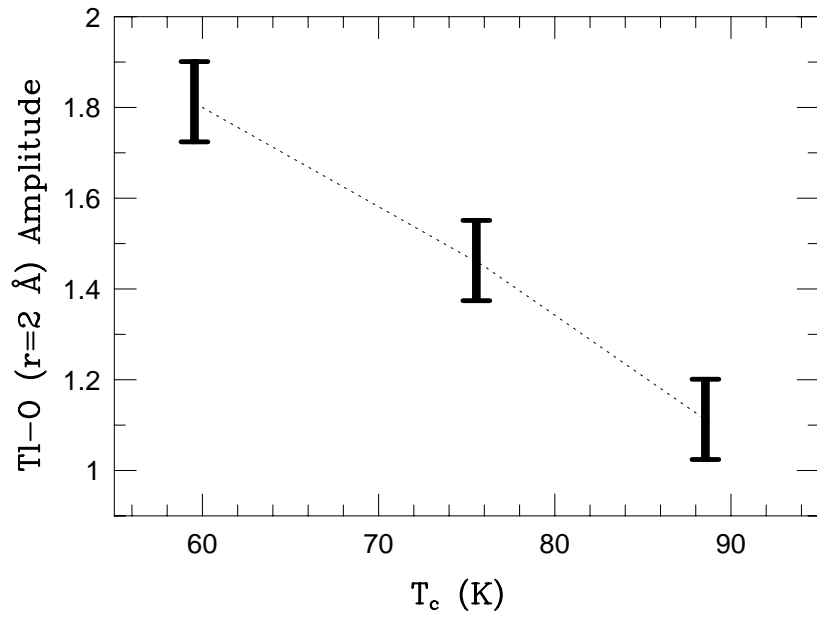


Second TiO layer









♂	♀	♂	♀	♂	♀	♂	♀	♂	♀	♂	♀
♀	♂	♀	♂	♀	♂	♀	♂	♀	♂	♀	♂
♂	♀	♂	♀	♂	♀	♀	♂	♀	♂	♀	♂
♀	♂	♀	♂	♀	♂	♂	♀	♂	♀	♂	♀
♀	♂	♀	♂	♀	♂	♀	♂	♀	♂	♀	♂
♂	♀	♂	♀	♂	♀	♂	♀	♂	♀	♂	♀

♂	♀	♂	♀	♂	♀	←○	○→	○→	←○	←○	○→
♀	♂	♀	♂	♀	♂	○→	←○	←○	○→	○→	←○
♂	♀	♂	♀	♂	♀	←○	○→	○→	←○	←○	○→
♀	♂	♀	♂	♀	♂	○→	←○	←○	○→	○→	←○
♀	♂	♀	♂	♀	♂	←○	○→	○→	←○	←○	○→
♂	♀	♂	♀	♂	♀	○→	←○	←○	○→	○→	←○